Cell Metabolism

Article

Hepatic lipid remodeling in cold exposure uncovers direct regulation of bis(monoacylglycero)phosphate lipids by phospholipase A2 group XV

Graphical abstract

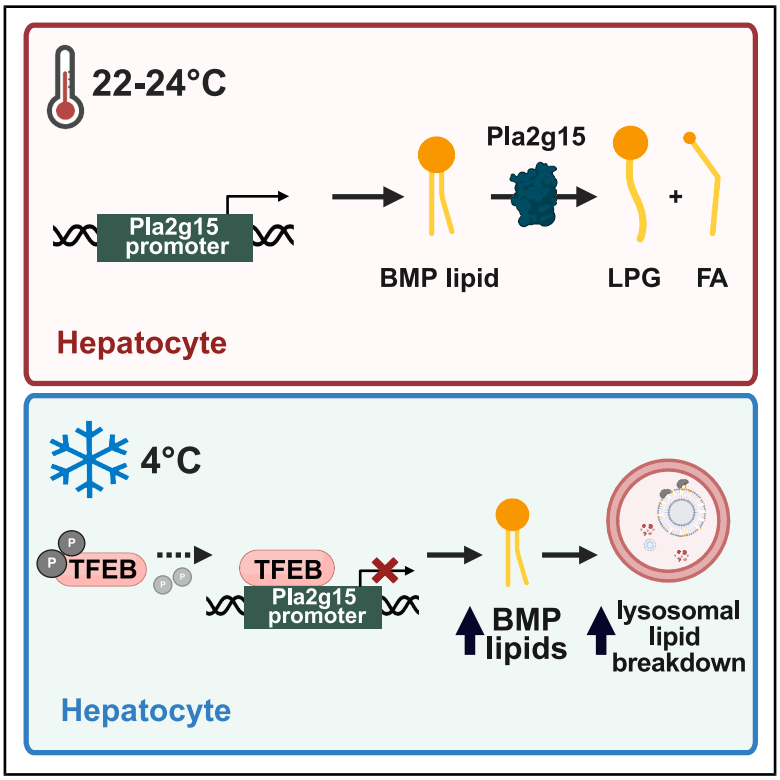

Authors

Jessica W. Davidson, Raghav Jain, Thomas Kizzar, ..., James A. Shayman, Monther Abu-Remaileh, Judith A. Simcox

Correspondence

jsimcox@wisc.edu

In brief

Davidson et al. demonstrated that liver lysosomes orchestrate the metabolic adaptation to cold by rewiring lipid processing. They show that phospholipase A2 group XV (PLA2G15) breaks down bis(monoacylglycerol) phosphate (BMP) lipids to shift lysosomal function and metabolism in response to direct transcription factor EB regulation.

Highlights

- Liver bis(monoacylglycerol)phosphate (BMP) lipids are increased with cold exposure
- BMP lipids regulate liver lysosomal function and metabolic adaptation to cold
- Phospholipase A2 group XV (PLA2G15) regulates BMP lipids in cold exposure
- PLA2G15 loss increases BMP lipids, lysosomal lipid processing, and energy expenditure

Davidson et al., 2025, Cell Metabolism *37*, 1413–1425
June 3, 2025
https://doi.org/10.1016/j.cmet.2025.04.015

CellPress

Cell Metabolism

CellPress
OPEN ACCESS

Article

Hepatic lipid remodeling in cold exposure uncovers direct regulation of bis(monoacylglycero)phosphate lipids by phospholipase A2 group XV

Jessica W. Davidson,[1,12] Raghav Jain,[1,2,12] Thomas Kizzar,[1] Gisela Geoghegan,[1] Daniel J. Nesbitt,[3] Amy Cavanagh,[1] Akira Abe,[4] Kwamina Nyame,[5,6,7] Andrea Hunger,[1] Xiaojuan Chao,[8] Isabella James,[1] Helaina Walesewicz,[1] Dominique A. Baldwin,[1,2] Gina Wade,[1] Sylwia Michorowska,[1,9] Rakesh Verma,[4] Kathryn Schueler,[1] Vania Hinkovska-Galcheva,[4] Evgenia Shishkova,[10] Wen-Xing Ding,[8] Joshua J. Coon,[3,10,11] James A. Shayman,[4] Monther Abu-Remaileh,[5,6,7] and Judith A. Simcox[1,2,13,*]

[1]Department of Biochemistry, University of Wisconsin-Madison, Madison, WI 53706, USA
[2]Howard Hughes Medical Institute, Department of Biochemistry, University of Wisconsin-Madison, Madison, WI 53706, USA
[3]Department of Chemistry, University of Wisconsin-Madison, Madison, WI 53706, USA
[4]Department of Internal Medicine, University of Michigan, Ann Arbor, MI 48109, USA
[5]Department of Chemical Engineering, Stanford University, Stanford, CA 94305, USA
[6]Department of Genetics, Stanford University, Stanford, CA 94305, USA
[7]The Institute for Chemistry, Engineering & Medicine for Human Health (Sarafan ChEM-H), Stanford University, Stanford, CA 94305, USA
[8]Department of Pharmacology, Toxicology and Therapeutics, University of Kansas Medical Center, Kansas City, KS 66160, USA
[9]Department of Drug Chemistry, Pharmaceutical and Biomedical Analysis, Faculty of Pharmacy, Medical University of Warsaw, Warsaw, Poland
[10]Department of Biomolecular Chemistry, University of Wisconsin-Madison, Madison, WI 53706, USA
[11]Morgridge Institute for Research, Madison, WI 53715, USA
[12]These authors contributed equally
[13]Lead contact
*Correspondence: jsimcox@wisc.edu
https://doi.org/10.1016/j.cmet.2025.04.015

SUMMARY

Cold exposure is a selective environmental stress that elicits a rapid metabolic shift to maintain energy homeostasis. In response to cold exposure, the liver rewires the metabolic state, shifting from glucose to lipid catabolism. By probing the liver lipids in cold exposure, we observed that the lysosomal bis(monoacylglycero)phosphate (BMP) lipids were rapidly increased during cold exposure. BMP lipid changes occurred independently of lysosomal abundance but were dependent on the lysosomal transcriptional regulator transcription factor EB (TFEB). Knockdown of *Tfeb* in hepatocytes decreased BMP lipid levels and led to cold intolerance in mice. We assessed TFEB-binding sites of lysosomal genes and determined that the phospholipase a2 group XV (PLA2G15) regulates BMP lipid catabolism. Decreasing *Pla2g15* levels in mice increased BMP lipids, ablated the cold-induced rise in BMP lipids, and improved cold tolerance. Mutation of the catalytic site of PLA2G15 ablated the BMP lipid breakdown. Together, our studies uncover TFEB regulation of BMP lipids through PLA2G15 catabolism.

INTRODUCTION

The liver maintains energy homeostasis in mammals by acting as a metabolic transistor switching between providing glucose or lipids for peripheral tissue catabolism. In the fed state, the liver is a sink for excess glucose to maintain normoglycemia. When nutrients are scarce in fasting, the liver processes and packages lipids to fuel peripheral tissues and reserve glucose for the brain. The shift to systemic lipid utilization is a coordinated response between multiple organs that begins with white adipose lipolysis of triglyceride stores, which releases free fatty acids into circulation, a portion of which are taken up by the liver and processed.[1–4] Understanding nutrient regulation in the liver during stress adaptation provides insight into how these processes are disrupted in the metabolic syndrome.[5]

One metabolic stress that causes rapid liver lipid remodeling is cold exposure.[6] Cold exposure is a selective pressure that increases white adipose tissue (WAT) lipolysis, with excess free fatty acids being taken up into the liver for processing into complex lipids; acute cold exposure leads to temporary hepatic steatosis.[7,8] Loss of this hepatic lipid processing in cold exposure leads to cold intolerance.[6,7] To identify other liver lipid metabolism pathways altered in cold exposure, we used untargeted liquid chromatography-mass spectrometry (LC-MS)-based

lipidomics. We identified over 200 liver lipid species that were significantly altered with cold exposure.[6,9] These lipids represented a variety of chemically distinct lipid classes including acylcarnitines, triglycerides, ceramides, and phospholipids. We also noted 94 spectral features from our LC-MS analysis that were not identified but had reproducible, temperature-dependent differences in abundance. We wanted to determine the identity of these features and explore their function in mediating nutrient regulation in the liver.

Through assessing spectral feature fragmentation, we determined that several of these cold-induced spectral features were bis(monoacylglycero)phosphate (BMP) lipids and validated these observations with targeted methods. BMP lipids are localized to the lysosome, where they mediate lipid and protein degradation.[10–12] Accumulation of BMP lipids is characteristic of a number of lysosomal disorders; however, their regulation and function remain poorly understood.[13–15] To determine if increased BMP lipids correlated with altered lysosomal function, we profiled lysosomes using imaging and biochemical assays. We observed that lysosomes were localized to lipid droplets during cold exposure and that transcription factor EB (TFEB), a regulator of autophagy and lysosomal biogenesis, exhibited a cold-induced activity shift contributing to altered lysosomal lipid metabolism.[16,17] Liver knockdown (KD) of *Tfeb* resulted in decreased BMP lipids and cold intolerance in mice. We determined that TFEB regulated BMP lipid levels through the lysosomal phospholipase A2 group XV (*Pla2g15*) in hepatocytes. Our findings shed new light on the processes that govern liver adaptation to acute cold and on the regulation of BMP lipids via TFEB and PLA2G15. These findings hold the potential to modulate BMP lipids for the treatment of lysosomal storage disorders and metabolic disease.

RESULTS

Lysosomal BMP lipids are increased in the liver during cold exposure in mice

To identify uncharacterized lipids that regulate liver fuel switching, we housed mice at room temperature (RT; 22°C–24°C) or cold (4°C) for 6 h with food removed at the start of the experiment. Liver lipids were extracted by an organic solvent mixture, and untargeted lipidomics by LC-MS was used to identify 712 lipids (Figures 1A and S1A). We observed that over 8,000 additional MS/MS spectra collected in the experiment remained unannotated (unidentified ''features''). To determine whether some of these features represented identifiable compounds important for survival in cold, we filtered the features to remove background ions and retained features that (1) had a retention time characteristic of lipids (1.0–15 min), (2) had a mass within the expected lipid range (400–1,500 m/z), and (3) were present in at least 80% of samples. This reduced the dataset to 1,233 unidentified features (Figure 1B). Next, we selected unidentified spectral features based on shared fragmentation patterns as well as the magnitude of fold change and significance between RT and cold using a false discovery rate (FDR) threshold of $q < 0.05$ (Figure 1C). Using the LIPIDMAPS database (https://www.lipidmaps.org), we determined that two of the most significantly increased features were BMP lipids, a class of lysosomal lipids (Figure S1B).

To validate this finding, we developed a targeted LC-MS method to quantify 42 BMP lipid species and their precursor lipid phosphatidylglycerols (PGs).[18] 14 individual BMP lipids were significantly increased in the liver during cold exposure with the majority containing essential fatty acids including 6 with an 18:2 acyl chain (Figures 1D and S1C). The 18:2 fatty acid is a polyunsaturated fatty acid that is associated with increased membrane fluidity, potentially indicative of changes in BMP lipid function. We did not observe changes in liver PGs (Figures S1D and S1E). Interestingly, circulating BMP ($p < 0.05$) and PG ($p < 0.01$) lipids were significantly decreased during cold exposure (Figure S1F). Time course studies demonstrated that the rise in BMP lipids predominantly occurs in the liver at 6 h (Figure 1E), but the elevation continues through a longer time course of 24 h post cold exposure (Figures 1F and S1G).

BMP lipids function as structural components of intralumenal vesicles within the endolysosomal system and are considered markers of lysosomal abundance. *In vitro* liposomal assays have demonstrated that polyunsaturation in BMP acyl chains facilitates BMP lipid interaction with lysosomal proteases and lipases, enhancing degradation of proteins and lipids in the lysosome lumen.[10,19] The specific rise in polyunsaturated fatty acid containing BMP lipids could indicate a functional shift in lysosomes during cold exposure, or simply reflect a rise in lysosomal abundance.

Lysosomes are localized to lipid droplets during cold exposure

To determine whether the increase in BMP lipids with cold exposure was driven by increased lysosomal abundance, we assessed organelle abundance and localization in liver sections using electron microscopy (Figure 2A). There was no change in lysosomal abundance; however, lipid droplet abundance and lysosomal localization to lipid droplets were increased with cold exposure (Figure 2B). Other notable shifts in liver morphology included elongated mitochondria. We also quantified lysosomal (LAMP1, LAMP2, RAB5, and LIPA) and autophagy (LC3-I and LC3-II) protein levels, which were unchanged, with the exception of LC3-II/-I and LAMP1, which had minor but significant increases with cold exposure (Figure 2C).[16,17] Transcripts for lysosomal markers were largely unchanged between RT and cold except *Hexa* and *Atp6v1h*, which were significantly increased with cold exposure, and *Lipa* and *Npc2*, which were decreased with cold (Figures 2D and S2A).

To determine whether the increased localization of lysosomes to lipid droplets coincided with a shift in function, we quantified lysosomal lipids in the liver using the LysoTag mouse[20] and cathepsin activity. Lysosomes are known to break down complex lipids including ceramides and glucosylceramides, with the activity of glucosylceramidases shifting in response to physiological stress such as fasting and high-fat diet.[21,22] Aligned with these observations, there was a significant decrease in glucosylceramide d18:1/24:1 with cold exposure and a trend in decreased d18:0/16:0, d18:0/24:1, and d18:1/16:0 glucosylceramides, which would indicate increased glucosylceramidase activity (Figure 2E). The isolated lysosomes also had the expected cold-induced increase in BMP lipids (Figure S2G). There were no changes in cathepsin B activity (Figure 2F). These results

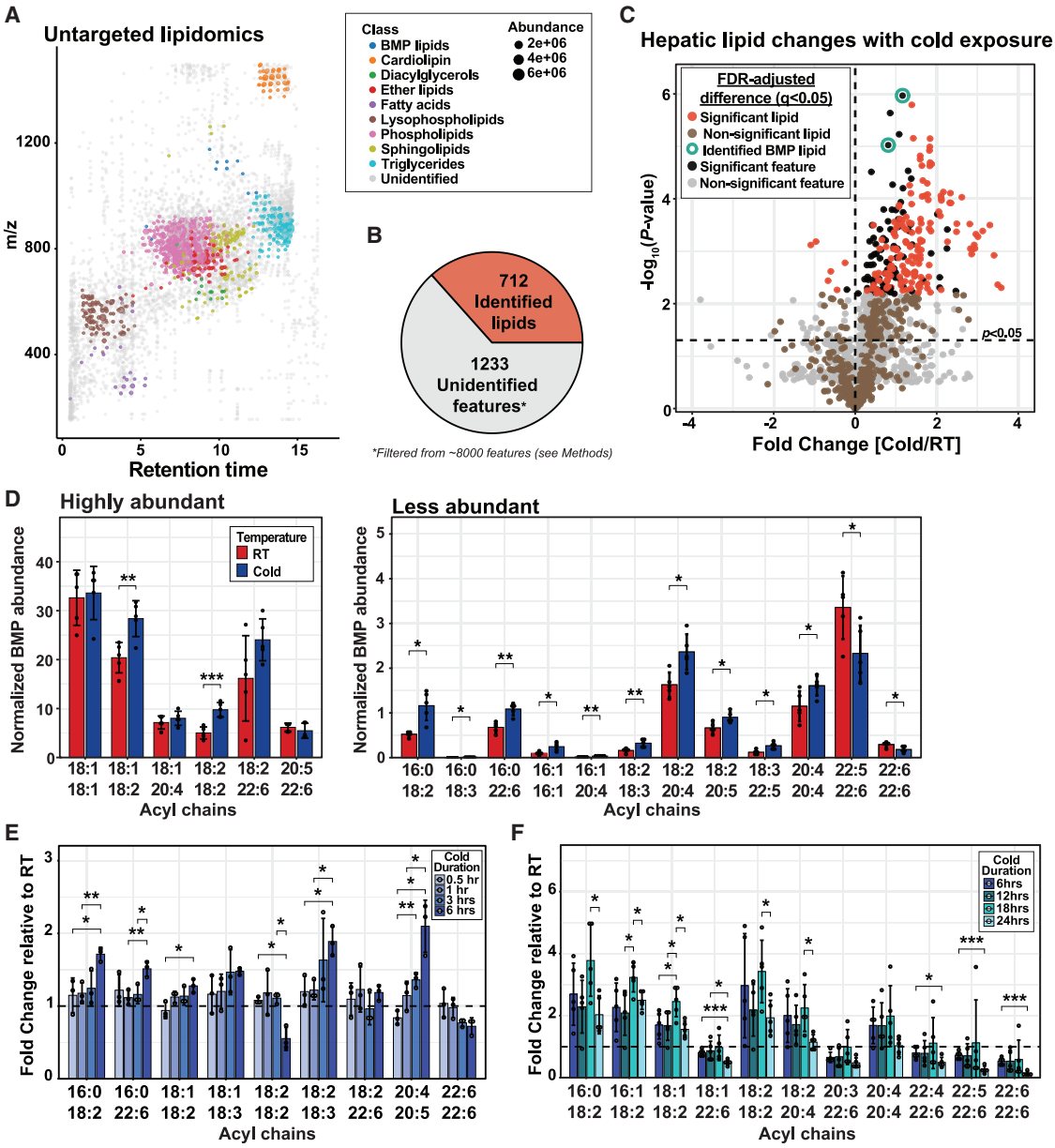

Figure 1. Lysosomal BMP lipids are increased in the liver during acute cold exposure in mice

(A) Untargeted LC-MS analysis of mouse liver plotted to size (m/z) versus retention time with each dot representing a molecular feature.

(B) Pie chart representing the number of identified lipids and unidentified lipid-like features. Total unidentified features (~8,000) were filtered to remove background ions and contaminants and retain features present in at least 80% of samples. Remaining features were further filtered based on the retention time of lipid elution (0.5–15 min) and mass-to-charge (m/z) range (200–1,500 m/z) of potential lipid species.

(C) Volcano plot of identified lipids and unidentified features (from B) comparing RT (24°C) with cold (4°C) in the liver after 6 h (n = 6 biological replicates/group). Points in red or black represent significantly altered lipids or features, respectively, after false-discovery correction (q < 0.05). Features circled in green were manually identified as lysosomal BMP lipid species based on the fragmentation pattern.

(D) Individual hepatic BMP lipid species were measured using a targeted LC-MS method in liver from RT and cold-exposed mice (6 h duration, n = 5 biological replicates/group). The acyl chain compositions of the BMP species are plotted on the x axes. The most abundant BMP species are plotted on the left and significantly altered (p < 0.05), less abundant BMP lipids are on the right.

(E) BMP lipid species changes in the liver during a short cold exposure time course of 0.5, 1, 3, and 6 h, plotted as fold change relative to RT (n = 3 biological replicates/group).

(F) BMP lipid species changes in the livers of cold-exposed mice for up to 24 h, reported as fold change relative to RT controls (n = 5/group).

Where relevant, mean ± SD of experimental groups is plotted. BMP lipid abundances were normalized to internal standards and tissue weight. Student's t test was used for significance testing to compare lipid values. *p < 0.05, **p < 0.01, ***p < 0.001. BMP, bis(monoacylglycero)phosphate; FDR, false discovery rate; LC-MS, liquid chromatography-mass spectrometry; RT, room temperature.

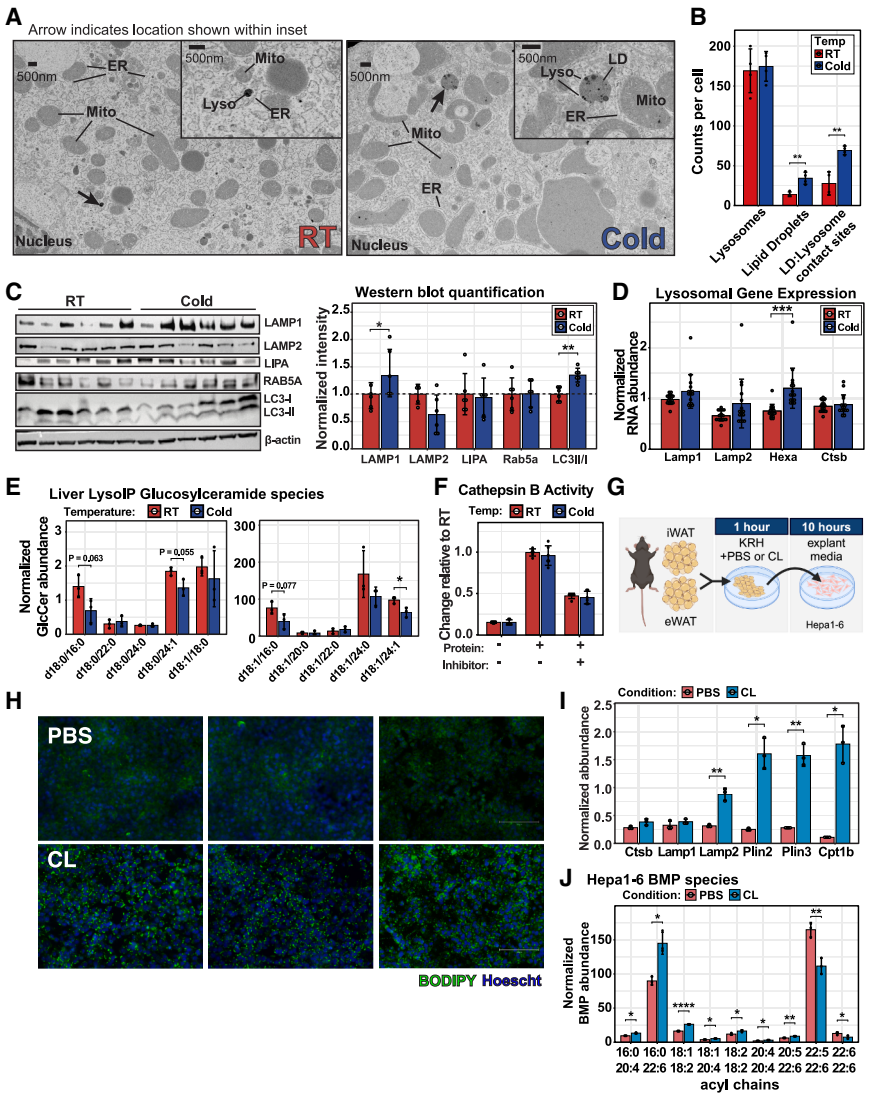

Figure 2. Lysosome localization is altered during cold exposure

(A) Electron micrographs of liver sections from mice kept at either RT or cold exposure. Lysosomes are visible as dark, electron dense organelles. Arrows indicate zoomed in regions within insets.

(B) Quantification of lysosomes, lipid droplets (LDs), and contact sites between lipid droplets and lysosomes.

(C) Western blot of lysosomal abundance and autophagy markers in liver from RT (24°C) and cold (4°C) exposed mice (n = 6 biological replicates/group). Densitometry based quantification was normalized to average RT signal, and Wilcoxon non-parametric test used to calculate p values.

(D) Lysosomal gene expression in liver from RT and cold-exposed mice, assessed by qPCR (n = 8 biological replicates/group; 2 technical replicates per biological replicate shown).

(E) Glucosylceramide species in the lysosomes within the liver of RT and cold-exposed LysoTag mice (n = 3 biological replicates/group).

(F) Comparison of lysosomal cathepsin B protease activity in liver from mice at kept at RT or cold (n = 6 biological replicates/group).

(G) Schematic of experimental design, mimicking cold exposure in Hepa 1–6 cells using adipose tissue isolated from mice and treated with CL-316,243.

(H) Bodipy and Hoescht staining of Hepa 1–6 cells incubated with explant media, in green and blue, respectively.

(I) Gene expression of lysosomal and lipid droplet markers, as well as *Cpt1b*, which is known to be induced by cold exposure in the liver (n = 3 biological replicates/condition, 2 technical replicates performed).

(J) Abundant BMP species that are significantly altered ($p < 0.05$) in the CL condition are plotted (n = 3 biological replicates/condition). All lipid measurements are normalized to internal standards.

Where relevant, mean ± SD of experimental groups is plotted. Student's t test was used for significance testing. *$p < 0.05$, **$p < 0.01$, ***$p < 0.001$, ****$p < 0.0001$. CL, CL-316,243; KRH, Krebs-Ringer buffer.

suggest a targeted shift in lysosomal activity, specifically toward lysosomal lipid processing.

One challenge in determining the mechanism of liver BMP lipid regulation in cold exposure is understanding the cells that contribute to the lipid phenotype. Recent work has shown that hepatocytes are the primary contributor to BMP lipids in the liver, and to confirm this, we used a culture model of hepatocytes (Hepa 1–6 cells).[23] The hepatocyte response to cold exposure is mediated by free fatty acid lipolysis in WAT.[6] To recapitulate this lipolysis, we treated WAT explants with β3-adrenergic receptor agonist CL-316,243 (CL) to induce lipolysis or vehicle control (PBS), and then transferred the media to the Hepa 1–6 cells (Figure 2G). We observed that Hepa 1–6 cells with CL explant treatment have increased lipid droplet abundance, similar to hepatocytes in the liver (Figures 2B and 2H). We observed increases in transcripts for lysosomal markers (*Lamp2*), lipid droplet markers (*Plin2* and *Plin3*), and an established mitochondrial marker responsive to cold exposure (*Cpt1b*) (Figure 2I).[6,16] We also observed a significant increase in specific BMP lipid species that corresponds to the changes we observed in the liver (Figure 2J). These results suggest that the major changes observed in the liver are driven by hepatocyte-specific differences in response to adipocyte lipolysis.

In total, biochemical analyses show increased lysosomal localization to lipid droplets with cold exposure and increased lysosomal lipid processing. These results also suggest that the differences in BMP lipids are driven by changes in hepatocytes and that these changes are in response to altered WAT lipolysis. We next sought to determine the regulation of these changes in lysosomal function and localization.

The master lysosomal regulator TFEB is activated during cold exposure

We evaluated liver transcript levels for genes involved in lysosome biogenesis and function as well as related processes including autophagy (*Gabarapl1* and *Sqstm1*), mitochondrial

CellPress
OPEN ACCESS

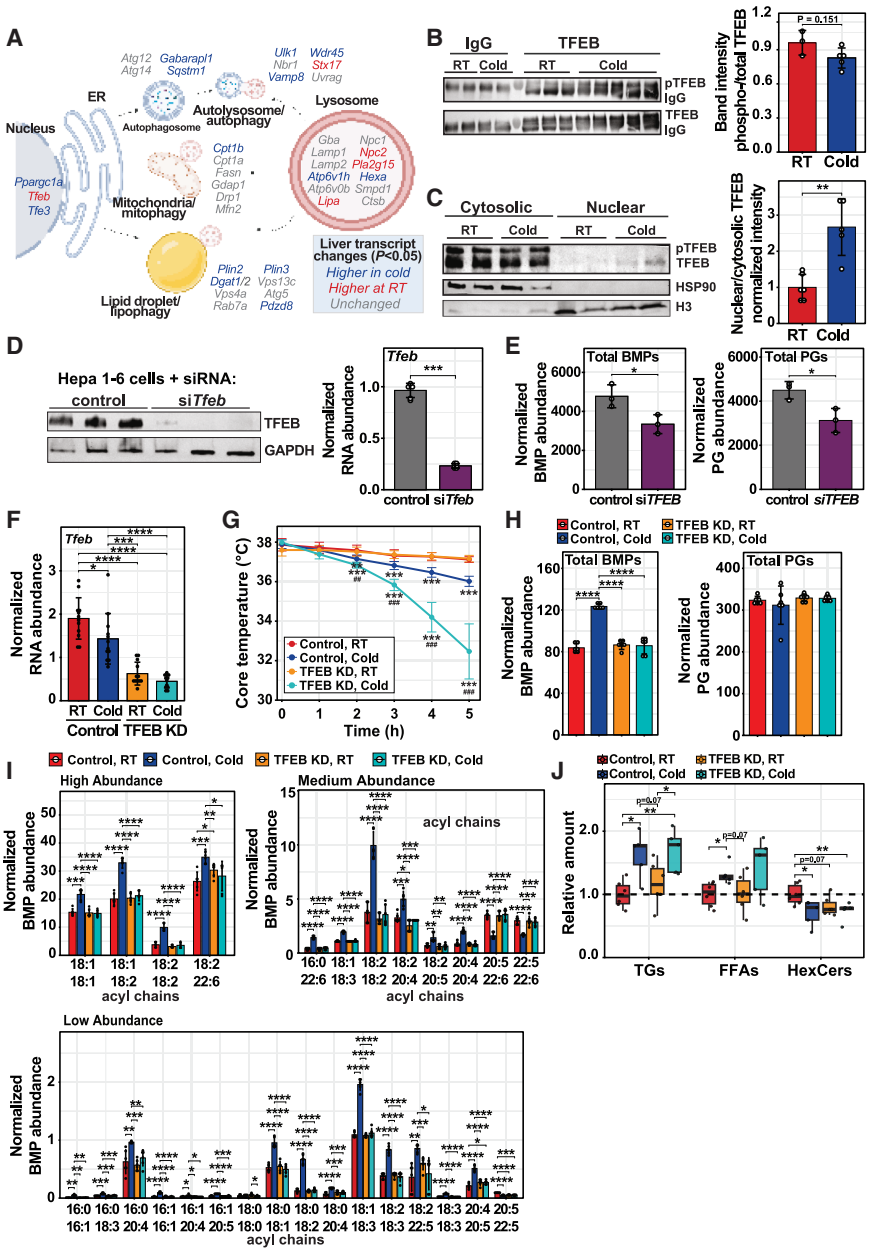

Figure 3. Hepatic KD of *Tfeb* causes cold intolerance in mice

(A) Schematic of potential lysosomal activities and associated genes for each process/organelle function. Genes are colored based on qPCR transcriptional changes ($p < 0.05$) between RT and cold-exposed murine livers ($n = 6$ biological replicates/group).

(B) TFEB immunoprecipitation and western blot of TFEB phosphorylation in the liver of RT ($n = 3$ biological replicates) and 6 h cold-exposed mice ($n = 5$ biological replicates). IgG was used as a control for the immunoprecipitation. The upper bands, representing phospho- (top blot) and total (bottom blot) TFEB, were quantified based on densitometry, and their ratio is reported.

(C) Western blot of TFEB from liver of mice kept at RT or cold ($n = 6$ biological replicates/group). Liver lysate was fractionated into nuclear and cytosolic fractions prior to western blot. Bands were quantified using densitometry and the ratio of nuclear (active) to cytosolic (inactive) TFEB signal was plotted.

(D) Western blot of TFEB protein in Hepa 1–6 cells treated with siRNA targeting *Tfeb* or a scramble sequence as control is shown ($n = 3$ technical replicates/condition). Gene expression of *Tfeb*, measured by qPCR, is to the right ($n = 3$ technical replicates/condition).

(E) Total BMP and PG lipids of Hepa 1–6 murine hepatocytes treated with siRNA against *Tfeb* or a scramble sequence control is plotted ($n = 3$ technical replicates/group). Lipids are normalized to internal standards and protein content.

(F) Hepatic *Tfeb* expression in mice treated with AAV8-GFP-U6-scrmb-shRNA (control; $n = 12$ biological replicates) or AAV8-GFP-U6-TFEB-shRNA (TFEB KD; $n = 12$ biological replicates), and exposed to 5 h of RT or cold 3 weeks after AAV injection.

(G) Core body temperature was measured hourly via rectal probe in control or TFEB KD mice kept at RT or cold for 5 h ($n = 6$ biological replicates/group). A two-way ANOVA with interaction was used to assess the effect of KD and environmental temperature on core body temperature. Asterisks (*) denote significant ($p < 0.05$) difference between core temperature due to environmental temperature of mice with the same KD status. Pound sign (#) indicates significant difference in core temperature between control and KD mice kept at 4°C.

(H) Total liver BMP lipids and PGs for each group from the cold tolerance test ($n = 6$ biological replicates/group), assessed by targeted lipidomics.

(I) BMP lipid species significantly altered during cold exposure are plotted ($n = 6$ biological replicates/group). Lipid abundances are normalized to internal standards and tissue weight.

(J) Lipid abundance of various lipid classes in the liver are measured by untargeted LC-MS lipidomics are plotted. Values are relative to RT controls for each lipid class. Where relevant, mean ± SD of experimental groups is plotted. *$p < 0.05$, **$p < 0.01$, ***$p < 0.001$, ****$p < 0.0001$. HexCer, hexosylceramide; BMP, bis(monoacylglycero) phosphate; FFAs, free fatty acids; PG, phosphatidylglycerol; KD, knockdown; RT, room temperature; TFEB, transcription factor EB; TGs, triglycerides.

oxidation (*Ppargc1a* and *Cpt1b*),[6,9] endosome (*Ulk1*, *Stx17*, and *Wdr45*), and lipid droplet formation (*Plin2*, *Dgat1*, *Pdzd8*, and *Plin3*) (Figures 3A and S2A–S2F). There were coordinated changes including increases in autophagy markers *Gabarapl1* and *Sqstm1*[24] and increases in lysosomal markers *Atp6v1h* and *Hexa* in cold. Many of these transcripts contain a coordinated lysosome expression and regulation (“CLEAR”) sites upstream and downstream of their promoters.[24,25] These sites are bound by transcription factors that are members of the microphthalmia-associated transcription factor (MiTF) family. The most abundant MiTF member in hepatocytes is TFEB.[26,27] There were also significant expression changes in *Tfeb* and *Tfe3* (Figure S2B). To determine whether there was altered TFEB activity, we assessed liver protein levels of phosphorylated and unphosphorylated TFEB observing a decrease in phosphorylation (Figure 3B) coinciding with increased nuclear (active) TFEB

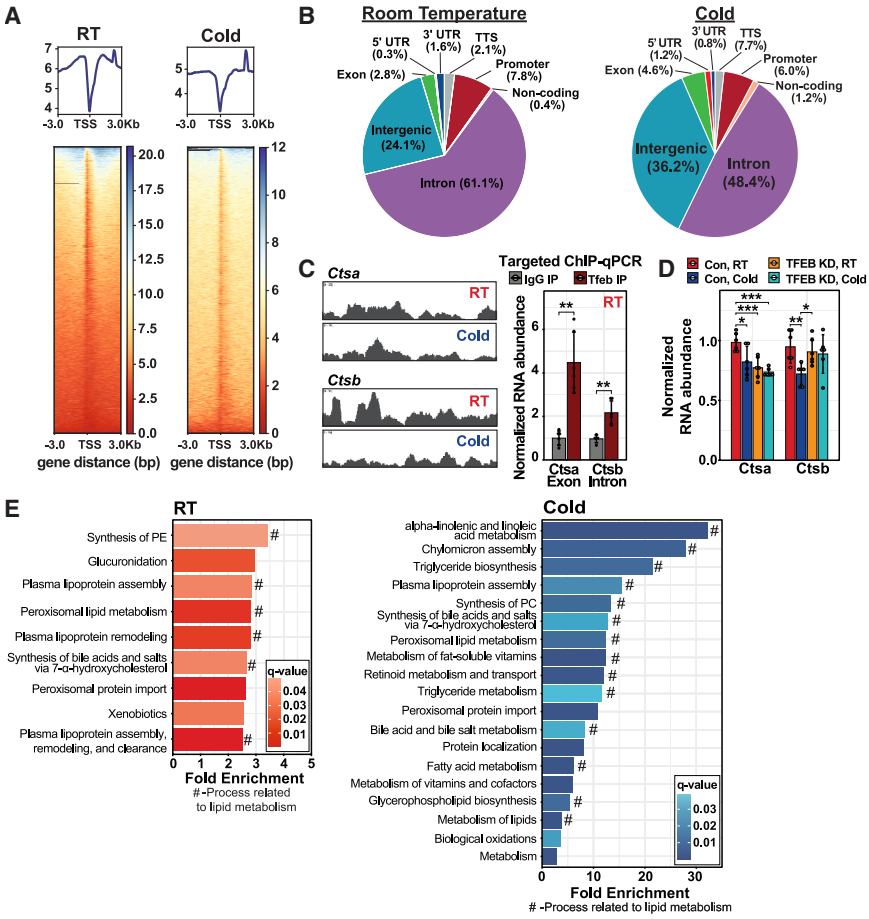

Figure 4. ChIP-seq of hepatic TFEB indicates a reprogramming of lipid metabolism during cold exposure

(A) Transcription-start-site-centered heatmaps comparing hepatic TFEB binding between RT and cold based on ChIP-seq data.

(B) Pie chart describing the distribution of TFEB genomic binding sites during RT or cold.

(C) ChIP tracks of previously described genes known to be bound by TFEB are shown.[13] Targeted ChIP-qPCR was performed to validate binding sites.

(D) Gene expression of *Ctsa* and *Ctsb* in the liver of control and TFEB KD mice kept at RT or exposed to cold for 6 h ($n = 6$ biological replicates/group, 2 technical replicates performed).

(E) Reactome of genes annotated to TFEB binding sites at RT or with 6 h of cold exposure. Of processes represented in the gene sets, those related to lipid metabolism are annotated with a "#." All ChIP analyses were performed after false-discovery correction with a $q < 0.05$ cutoff.

Where relevant, mean ± SD of experimental groups is plotted. $^{*}p < 0.05$, $^{**}p < 0.01$, $^{***}p < 0.001$. ChIP-seq, chromatin immunoprecipitation sequencing; RT, room temperature; Con, control; TSS, transcription start site.

with cold exposure compared with cytosolic (inactive) TFEB (Figure 3C). The nuclear-to-cytosolic ratio of TFEB was 3-fold higher in cold than RT ($p < 0.01$; Figure 3C). Though most studies of TFEB activity characterization have focused on lysosomal activation, previous work has implicated TFEB in the control of hepatic lipid metabolism, including through activation of *Ppargc1a* (Figure S2B).[17,28]

To determine whether *Tfeb* modulated BMP lipids in hepatocytes, we used siRNA to knock down *Tfeb* in Hepa1–6 cells (Figure 3D). Controls were treated with siRNA containing a scramble sequence. After 48 h, cells were harvested for BMP analysis. Total BMP lipids were significantly decreased in *Tfeb* KD cells as were PG levels ($p < 0.05$; Figures 3E and 3F). The KD of *Tfeb* in fed mice led to decreased BMP lipid levels in the liver (Figure S3A). These results identified TFEB as a novel genomic regulator of BMP lipids in hepatocytes. Given the increase in nuclear-localized TFEB and regulation of BMP lipids by TFEB in hepatocytes, we aimed to determine whether TFEB was functionally important in cold tolerance and the hepatic lipid response.

Hepatic TFEB is required for cold tolerance in mice

To assess the requirement of hepatic TFEB in the cold response, we knocked down *Tfeb* using shRNA encoded in an AAV8 vector which targets hepatocytes. After 3 weeks, control and KD mice were subjected to 5 h at RT (23°C; $n = 5$–6 and 6, respectively), or 5 h in cold (4°C; $n = 5$–6 and 6, respectively) with food removed at the start of the experiment. In the liver, KD mice had ~70% lower *Tfeb* gene expression than controls (Figure 3F). Mice kept at 4°C had significantly lower core body temperature than those at RT after 2 h. Decreased body temperature in the cold was exacerbated with loss of TFEB ($p < 0.01$ at all time points; Figure 3G). Loss of TFEB also ablated cold-induced differences in BMP lipids (Figures 3H and 3I), but changes in other lipids persisted with loss of TFEB (Figures 3J, S3C, and S3D). Despite the major shift in body temperature with loss of TFEB, there were no changes between control and KD in body weight loss or transcripts associated with lipid droplets and mitochondria (Figures S3B–S3E). KD of TFEB did lead to increased liver weight and shifts in lysosomal transcripts (Figures S3B, S3F, and S3G). These results show that hepatic TFEB is required for acute cold adaptation in mice and that this regulation leads to altered lysosomal transcripts and BMP lipids, without major changes in other hepatic or circulating lipids.

Altered TFEB DNA occupancy influences lipid metabolism in cold exposure

Given the impact of liver TFEB loss on cold tolerance and BMP lipids, we sought to understand how TFEB regulates BMP lipids. Because TFEB is a transcriptional regulator, we performed chromatin immunoprecipitation sequencing (ChIP-seq) for TFEB in liver of mice housed at RT or fasted in cold for 6 h (Figures 4A and S4A). After filtering reads using a stringent FDR, we observed that there was a drastic shift in the type of binding sites between conditions. The percentage of intronic binding sites (of total sites) decreased from 61.1% in RT to 48.4% in cold

($q < 0.05$; Figure 4B). The majority of binding sites were for protein-coding genes, and the greatest increase was for intergenic regions (RT 24.1% to cold 36.2%), whereas the percentage of promoter-binding sites were similar in both conditions (RT 7.8% and cold 6.0%) (Figure S4B). We validated these results observing TFEB binding to established targets such as *Ctsa*, *Ctsb*, and *Npc1* (Figures 4C and S4C).[24] This was confirmed using targeted ChIP-qPCR based on binding sites annotated to TFEB from sequencing data (Figure 4C). These differences in TFEB activity may be driven by a shift in TFEB-binding partners as observed by LC-MS of TFEB co-immunoprecipitation (Figure S4D). The regulation by TFEB was confirmed by ablation of the cold-induced decrease in *Ctsa* and *Ctsb* expression in TFEB KD mouse livers (Figure 4D).

To identify the processes coordinated by TFEB in cold, we performed Reactome analysis using genes annotated to TFEB in cold as input and compared them with RT. We observed that 75% of all reported Reactome processes were related to lipid metabolism (Figure 4E). Many of the most significantly ($q < 0.05$) enriched processes were 10- to 30-fold above expected representation in the gene set. With our findings from TFEB KD mice, these data indicated that TFEB contributes to cold-induced alterations in hepatic lipid metabolism.

TFEB regulates BMP lipids via *Pla2g15* in hepatocytes *in vitro*

Due to the altered BMP lipid levels in TFEB KD hepatocytes, we postulated that TFEB regulates enzymes directly involved in the metabolism of BMP lipids in hepatocytes. To identify potential enzymatic BMP lipid regulators in the lysosome, we overlaid all unique genes identified in our TFEB ChIP-seq analysis with proteins localized to the lysosome,[20,29–31] and genes with expression significantly altered in cold exposure compared with RT after 6 h ($q < 0.05$; Figure 5A). We filtered the resulting list of 24 genes to 4 candidates that are predicted to be regulators of lipid metabolism (Figure 5A). Of these genes, only one had altered expression in cold and in TFEB KD cells, *Pla2g15* (Figures 5B and 5C). *Pla2g15* expression and protein levels were decreased with cold exposure (Figure 5D). There was a sharp peak upstream of the promoter of *Pla2g15* in both TFEB and RNA pol ChIP-seq—indicative of active transcription in RT. Targeted ChIP confirmed TFEB binding to the *Pla2g15* site (Figure 5E). There was also a CLEAR site present within the coding sequence 1,543 base pairs downstream of the transcription start site (sequence: GTCACGTGTG).[25] Luciferase assays of the TFEB-binding sites demonstrated TFEB occupancy of the *Pla2g15* promoter, which was increased in TFEB overexpression (Figures 5F and S5A).

To determine whether *Pla2g15* regulates BMP lipid levels, we performed a KD in Hepa 1–6 cells using siRNA (Figure 5G). KD of *Pla2g15* led to an increase in BMP lipids including BMP 18:1_18:2, one of the primary BMP lipids increased *in vivo* with cold exposure. Together, these data suggest that TFEB is a genomic regulator of *Pla2g15*, and that PLA2G15 may enzymatically regulate BMP lipids.

Pla2g15 is responsible for the cold-induced changes in BMP lipids

We propose a model in which TFEB binding to the *Pla2g15* promoter is inhibitory and PLA2G15 degrades BMP lipids into lysophosphatidylglycerol and fatty acids (Figures 6A and 6B). During cold exposure, increased TFEB binding of the *Pla2g15* promoter would decrease PLA2G15 expression, leading to the observed increase in BMP lipid levels. To directly test whether PLA2G15 regulates the cold-induced changes in BMP lipids, we knocked down *Pla2g15* in the livers of mice (Pla2g15 KD, AAV8-shPla2g15) (Figures 6C and S6A). *Pla2g15* KD led to improved cold tolerance, with mice better able to maintain their body temperature (Figure 6D). To ensure that the changes we observed were driven by hepatocytes, we isolated hepatocytes and confirmed that BMP lipids were increased with loss of *Pla2g15* (Figures 6A, 6E, 6F, S6B, and S6C). The improved cold tolerance with *Pla2g15* KD coincided with a loss of cold-induced increases in BMP lipids (Figures 6E, 6F, S6D, and S6E). Interestingly, loss of *Pla2g15* also ablated other cold-induced changes in liver lipids observed including ceramides, lysophosphatidylcholine, free fatty acids, hexosylceramides, and ether lipids (Figure 6G).

PLA2G15 is a BMP lipid phospholipase

To confirm that PLA2G15 is acting as a phospholipase to directly catabolize BMP lipids, we prepared liposomes containing the commercially available di-oleoyl BMP with non-hydrolyzable ether lyso-PC 18:0 in an acidic buffer to mimic the lysosome environment. We then added purified human PLA2G15 protein treated with or without the catalytic serine inhibitor diisopropyl fluorophosphate (DFP) and monitored for the degradation product oleic acid via TLC (Figure 7A). Fluorophosphonates such as DFP block the catalytic serine residue of PLA2G15 and inhibit activity.[32,33] In the presence of DFP inhibitor, there was no migration band related to oleic acid; however, in the reactions of liposomes and PLA2G15 only, there was a band characteristic of oleic acid, indicating degradation of di-oleoyl BMP (Figure 7A).

Phospholipase A2 enzymes contain a catalytic triad of a serine, histidine, and aspartic acid that facilitates the hydrolysis of the ester bond typically in the sn-2 position.[34,35] To determine whether PLA2G15 was directly acting on BMP lipids through this catalytic site, we mutated serine 165 to an alanine to generate a catalytically dead PLA2G15 (dPla2g15). Wild-type murine PLA2G15 and dPla2g15 were expressed in bacteria, isolated, and then incubated in liver lysate from cold-exposed mice for 15 min. PLA2G15 incubation led to a decrease in endogenous BMP lipids and PG, while dPla2g15 did not alter BMP lipid levels (Figures 7B and S7A). We also generated *Pla2g15* knockout (KO) in 293T cells and rescued expression with a Cas9 resistant *Pla2g15*− although expression was only partially restored (Figures 7C and 7D). Loss of *Pla2g15* increased total BMP lipid species (Figure 7E), and rescue with Cas9 resistant *Pla2g15* decreased several BMP lipids including 18:1_18:1 and 18:0_18:1 (Figure S7B).

To determine whether *Pla2g15* KO directly altered liver BMP lipid levels, we assessed control (*Pla2g15*$^{+/+}$) and KO (*Pla2g15*$^{-/-}$) mice.[36,37] Because this is a whole-body KO and there can be compensation, we re-expressed *Pla2g15* in hepatocytes alone with hepatocyte-specific driver thyroxine-binding globulin (AAV8-TBG Pla2g15) 3 weeks before cold exposure (Figures 7F and 7G). Mice were placed in cold for 6 h to increase BMP lipids. *Pla2g15* KO mice had elevated BMP lipid levels relative to their littermate controls, and re-expression of *Pla2g15* in

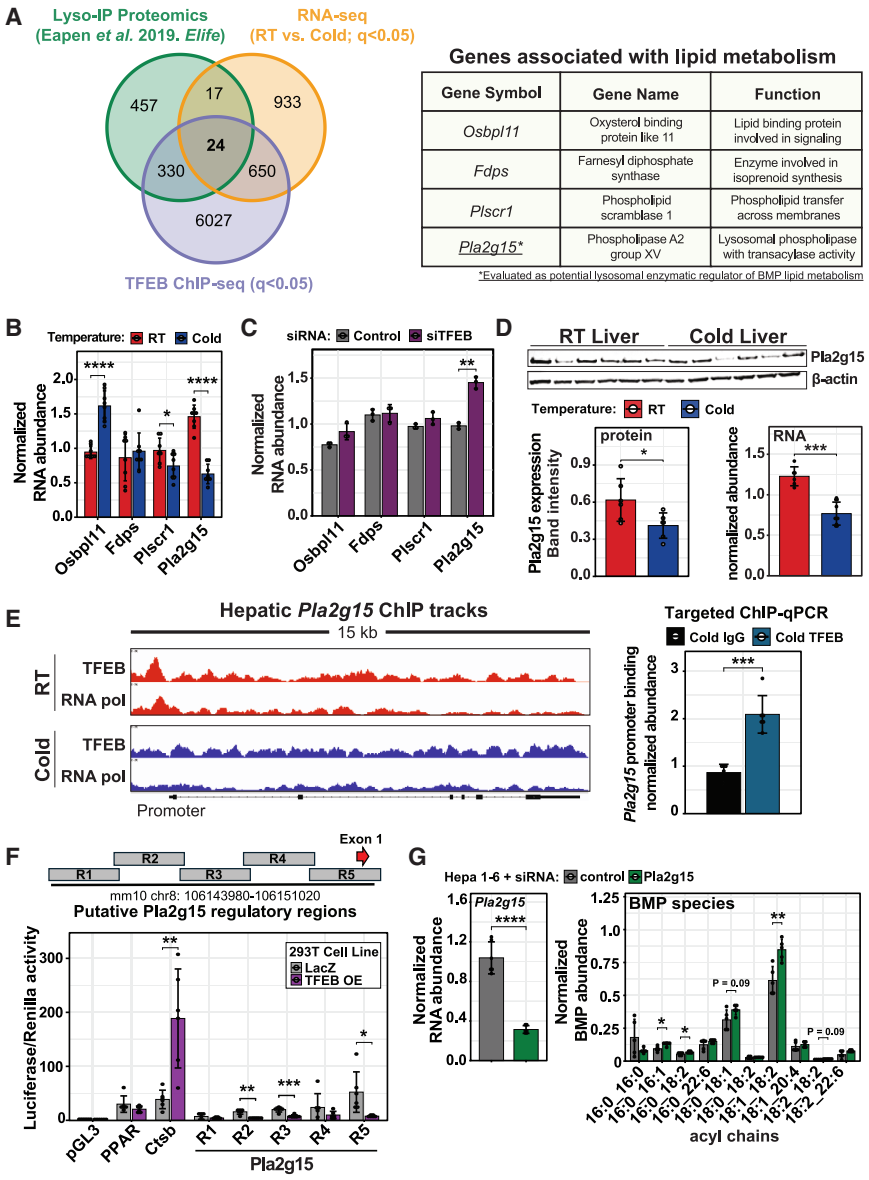

Figure 5. TFEB regulates BMP lipids in hepatocytes via *Pla2g15 in vitro*

(A) Overlay of identified lysosomal proteins[30] with all unique genes from TFEB ChIP-seq ($q < 0.05$) and all genes with expression significantly altered between RT and cold after 6 h ($q < 0.05$). Of the 24 genes in the center overlap, four were annotated with lipid functions and are shown in the table to the right.

(B) Expression of the candidate genes in liver from mice kept at RT or cold exposed for 6 h is shown ($n = 8$ biological replicates/group).

(C) Candidate gene expression in Hepa 1–6 cells treated with siRNA against *Tfeb* or a scrambled control ($n = 3$ biological replicates/group, 2 technical replicates performed).

(D) Western blot of PLA2G15 is shown for RT and cold-exposed mice ($n = 6$ biological replicates/group). Band intensity, normalized to the loading control b-actin, is plotted. Gene expression, measured by qPCR, is also shown for *Pla2g15* in RT and cold-exposed livers ($n = 6$ biological replicates/group).

(E) ChIP tracks of TFEB and RNA polymerase on the genomic region encoding *Pla2g15* in RT and cold livers. To the right, targeted ChIP-qPCR is shown for the binding regions of TFEB to the promoter of *Pla2g15* in the cold. IgG was used as a control.

(F) Schematic of *Pla2g15* regulatory regions expressed upstream of luciferase in LacZ or TFEB overexpressing 293T cells, in the luciferase-binding assay below. Luciferase activity was normalized to Renilla as a control ($n = 6$ technical replicates/condition, representative result from 3 independent experiments).

(G) Gene expression of *Pla2g15* in Hepa 1–6 cells treated with siRNA targeting *Pla2g15* or scramble sequence as control ($n = 3$ technical replicates/group, 2 replicates per sample). Select BMP lipid species were measured from Hepa 1–6 cells following treatment with siRNA against *Pla2g15* or a scramble sequence control ($n = 5$ biological replicates/group). Lipids normalized to internal standards and protein.

Mean ± SD of experimental groups is plotted. $^{*}p < 0.05$, $^{**}p < 0.01$, $^{***}p < 0.001$, $^{****}p < 0.0001$. BMP, bis(monoacylglycero)phosphate; TFEB, transcription factor EB.

hepatocytes decreased BMP lipid levels (Figures 7G, 7H, and S7C).

DISCUSSION

The response to cold exposure is metabolically challenging and requires coordination of metabolism across multiple organs. The liver plays a central role in the thermogenic response, altering lipid metabolism to fuel heat production.[1,6,8] Through lipidomics on the liver, we and others were able to determine that BMP lipids are increased during cold exposure.[23] Our studies determined that the rise in BMP lipids is driven by inhibition of Pla2g15, a BMP lipase that is transcriptionally controlled by TFEB. During cold exposure TFEB has altered DNA occupancy, predominantly regulating genes associated with lipid metabolism. We also observed an increase in PLA2G15 protein levels and a decrease of BMP lipids in the liver of TFEB KD mice exposed to cold coinciding with cold intolerance. Together, these studies provide new insights into liver thermoregulatory processes and the regulation of BMP lipids. BMP lipid levels are altered in a number of human diseases including hepatic steatosis and lysosomal storage disorders, although the regulation of BMP lipids in these diseases is poorly understood.[35,36,38]

There has been a resurgence in BMP lipid research since their initial characterization in 1967. This resurgence has been driven by improved methods to detect BMP lipids,[39–41] the potential for BMP lipids to serve as biomarkers of metabolic and neurodegenerative disease,[23,38,42,43] and the understanding that BMP lipids regulate lysosomal function. In the past 2 years, CLN5

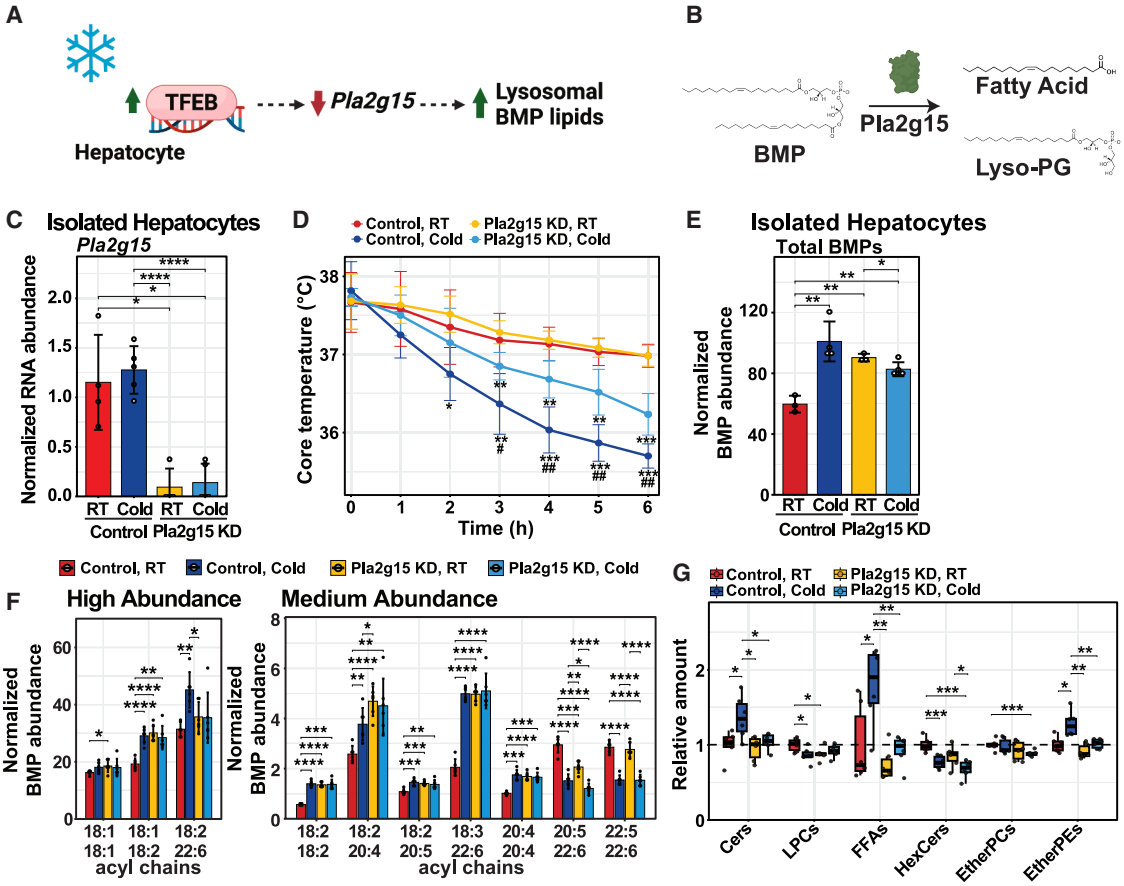

Figure 6. *Pla2g15* is responsible for cold-induced changes in BMP lipids

(A) Model summarizing the regulation of BMP lipids by TFEB and *Pla2g15*.

(B) Proposed mechanism of Pla2g15 degradation of BMP lipids.

(C) *Pla2g15* gene expression in hepatocytes isolated from mice 3 weeks post treatment with AAV8-GFP-U6-scrmb-shRNA (control; $n = 9$) or AAV8-GFP-U6-mPla2g15-shRNA (Pla2g15 KD; $n = 9$ biological replicates) and immediately following 6 h at either RT ($n = 4$ biological replicates/group) or cold ($n = 5$ biological replicates/group).

(D) Results of a cold tolerance test in control and Pla2g15 KD mice kept at RT or in the cold for 6 h, where core body temperature was recorded hourly ($n = 6$ biological replicates/group). A two-way ANOVA with interaction was used to assess the effect of *Pla2g15* KD and environmental temperature on core body temperature. Significant differences ($p < 0.05$) in core temperature due to environmental temperature of mice within the same group (Pla2g15 KD or controls) are indicated by asterisks (*). Significant differences in core temperature between the control and KD mice in the cold (4°C) are indicated by a pound sign (#).

(E) Total BMP lipids in hepatocytes isolated from control mice kept at RT or cold ($n = 3$ and $n = 4$ biological replicates, respectively) and Pla2g15 KD mice kept at RT and cold for 6 h ($n = 3$ and $n = 5$ biological replicates, respectively).

(F) Most abundant BMP lipid species that are significantly altered in whole liver with cold exposure are shown. BMP lipid abundances are normalized to internal standards and tissue weight.

(G) Lipid abundance in whole liver across several classes are reported, as measured by untargeted lipidomics. Abundances are relative to RT controls for each lipid class.

Data reported as mean ± SD of experimental groups. *$p < 0.05$, **$p < 0.01$, ***$p < 0.001$, ****$p < 0.0001$. Cers, ceramides; LPCs, lysophosphatidylcholines; HexCers, hexosylceramides; BMP, bis(monoacylglycero)phosphate; FFAs, free fatty acids; KD, knockdown; RT, room temperature; TFEB, transcription factor EB; TGs, triglycerides.

and PLD3/4[44–46] have been established as regulators of BMP lipid synthesis and are important in esterification of lysophosphatidylglycerol to BMPs. Our work adds to this growing exploration by functionally characterizing PLA2G15 as an enzyme capable of degrading BMP lipids and establishes regulation of *Pla2g15* by TFEB. Understanding mechanisms to regulate BMP lipid levels can yield therapeutic potential since treatment of NPC1-deficient cells with BMP lipids alleviates cholesterol burden and reduces cellular toxicity, which are characteristic of NPC diseases.[47,48]

PLA2G15 was originally identified as a lyso-phosphatidylcholine lipase and a transacylase that catalyzed the formation of 1-O-acylceramides from sn-2 fatty acyl groups.[36,37,49] In the absence of ceramide acceptors, PLA2G15 exhibits phospholipase activity against a wide range of glycerophospholipids and oxidized phospholipids.[37,50,51] The enzyme contains a core α/β-hydrolytic domain and catalytic triad consisting of Ser165, Asp327, and His359. The potential for PLA2G15 to regulate BMP lipids was first established by a recent study that identified it as a putative phosphatidylglycerol deacylase

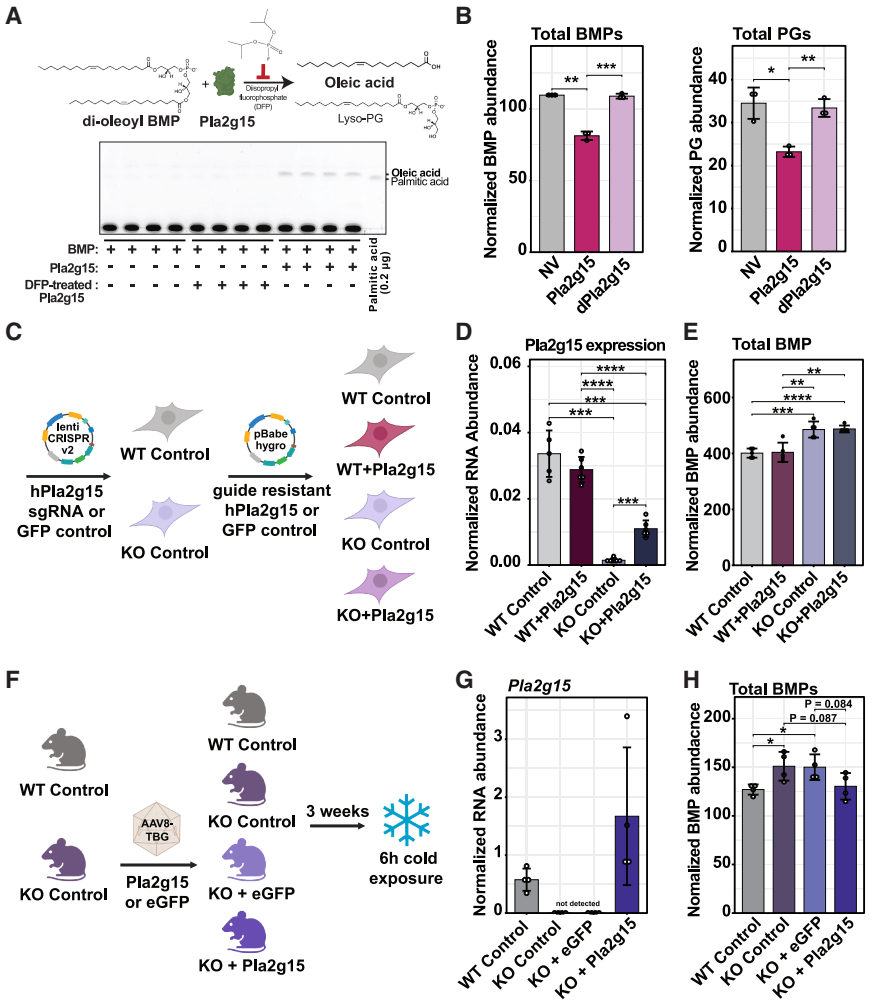

Figure 7. PLA2G15 degrades BMP lipids *in vivo*

(A) Schematic of an *in vitro* liposome assays using commercially available di-oleoyl BMP that was used to assess PLA2G15 activity (top). The expected products from PLA2G15 degradation of di-oleoyl BMP are oleic acid and lysophosphatidylglycerol (LPG). The PLA2G15 inhibitor DFP was used as negative control. In the present solvent system (see method details), one of the products, oleic acid, migrated onto the plate and was detected after release from BMP (n = 4 technical replicates/group).

(B) Total BMP lipid and PG abundance in liver lysates from mice exposed to cold for 6 h and then incubated with bacterially expressed PLA2G15 or catalytically dead PLA2G15 (dPla2g15; n = 3 biological replicates/group). Bacteria expressing no vector (NV) were used as a control.

(C) Experimental design for generating Pla2g15 KO 293T cells and overexpressing *Pla2g15* in the KO background.

(D) *Pla2g15* gene expression is shown for the *Pla2g15* KO, re-expression, and control cell lines described in (C) (n = 5 technical replicates/group).

(E) Total BMP lipid abundance measured in 293T cells with Pla2g15 KO and overexpression.

(F) Schematic of experimental design for overexpressing *Pla2g15* via AAV8-TBG in wild type (WT) and mice lacking *Pla2g15* (KO). 3 weeks post AAV injection, mice were kept at cold (4°C) for 6 h (n = 4 biological replicates/group).

(G) Hepatic expression of *Pla2g15* are plotted for the mice described in (F), after exposure to 6 h of cold.

(H) Total BMP lipids are reported, as measured by targeted lipidomics in the livers of control and Pla2g15 KO mice treated with an eGFP control or Pla2g15 AAV and exposed to cold for 6 h. Lipids are normalized to internal standards and tissue weight. When relevant, mean ± SD is plotted. *p < 0.05, **p < 0.01, ***p < 0.001, ****p < 0.0001. DFP, diisopropyl fluorophosphate; BMP, bis(monoacylglycero)phosphate; PG, phosphatidylglycerol; NV, no vector; dPla2g15, catalytically dead Pla2g15; WT, wild type; KO, knockout.

that contributes to BMP synthesis in HeLa cells.[52] More recent work identified and enzymatically characterized PLA2G15 as a BMP phospholipase using BMP lipid standards, which we were able to recapitulate.[53] Our work and the work of the Abu-Remaileh lab utilized assays in liver lysate to demonstrate that PLA2G15 is a BMP phospholipase.[51] We confirmed these results in multiple cell models, *Pla2g15* KO mice, and in *Pla2g15* KD mice. While our studies indicate a potential function of elevated BMP lipids in energy homeostasis in *Pla2g15* KD mice having improved cold tolerance, the Abu-Remaileh lab further went on to characterize the importance of PLA2G15 in lysosomal storage disorders.

There are over 300 single-nucleotide variants that have been characterized for *Pla2g15*[54]; additional work to understand PLA2G15 function and regulation will be crucial for the exploration of metabolic health and lysosomal storage disorders. Evidence is emerging that PLA2G15 may be important in autophagy,[55,56] lysosomal storage disorders,[51,57] and energy homeostasis. Further exploration of the mechanism by which TFEB activity is altered to regulate *Pla2g15* and the development of agonists for PLA2G15 are needed to probe the therapeutic potential of these discoveries.

Limitations of the study

Here, we have shown that lysosomal lipase PLA2G15 is transcriptionally suppressed by TFEB during cold exposure, leading to a rise in hepatic BMP lipid levels. These studies have several limitations. The majority of the work was performed in male mice. We have recapitulated some of these phenotypes in females (Figure S1); however, further studies are needed to determine whether there are sex specific differences in PLA2G15 function and regulation by TFEB. When possible, we used targeted genetic manipulation of TFEB and PLA2G15 in the liver to minimize systemic effects and developmental compensation. However, KD of these genes may influence other factors that contribute to the regulation of BMP lipids. While we observe differences in TFEB localization and phosphorylation, more work is needed to understand the mechanism of TFEB regulation in cold exposure. Similarly, the regulation of PLA2G15 remains elusive, whether post-translational modifications, substrate availability,

or cofactors affect PLA2G15 activity and BMP specificity remains unknown. The focus of this work was on demonstrating PA2G15 function as a BMP lipase that is transcriptionally regulated by TFEB during cold exposure.

RESOURCE AVAILABILITY

Lead contact

Requests for further information and resources should be directed to and will be fulfilled by the lead contact, Judith Simcox (jsimcox@wisc.edu).

Materials availability

This study did not generate new unique reagents. Mice were previously generated and described.[20,36]

Data and code availability

All original code associated with data processing has been deposited to GitHub (RJain52/Hepatic-TFEB). Lipidomics data have been deposited to MassIVE (MSV000096791), and all ChIP-seq data have been deposited to GEO (GSE292817).

ACKNOWLEDGMENTS

We thank Edrees H. Rashan, CiJi Lim, and Alan Attie for advice on experimental design and all Simcox Lab members for assistance with mouse experiments, editing materials, and thoughtful discussions. We also thank the Lim Lab at the UW-Madison for equipment use in protein isolation. The author(s) utilized the University of Wisconsin-Madison Biotechnology Center Bioinformatics Core Facility (RRID: SCR_017799) for analysis of the ChIP-seq data. M.A.-R. is a Stanford Terman Fellow and a Pew-Stewart Scholar for Cancer Research, supported by the Pew Charitable Trusts and the Alexander and Margaret Stewart Trust. K.N. is supported by the Sarafan ChEM-H Chemistry/Biology Interface Program as Kolluri Fellow. K.N. is additionally supported by the Bio-X Stanford Interdisciplinary Graduate Fellowship affiliated with the Wu Tsai Neurosciences Institute (Bio-X SIGF: Mark and Mary Steven's Interdisciplinary Graduate Fellow). J.A. Simcox is an HHMI Freeman Hrabowski Scholar. Research reported in this publication was supported by the Glenn Foundation and American Federation for Aging Research (A22068 to J.A. Simcox); Hatch Grant (WIS04000-1024796 to J.A. Simcox and R.J.); JDRF (JDRF201309442 to J.A. Simcox); an R01 through NIH/NIDDK (R01DK133479 to J.A. Simcox); the Dr. Stephen Babcock AG Chem Fellowship (I.J., G.W., and A.H.); and NIH (P41 GM108538 to J.J.C.). This material is based upon work supported by the National Science Foundation Graduate Research Fellowship program under grant nos. DGE-2137424 to J.W.D. and DGE-1747503 to H.W., support of the NIH/NIGMS funded Biotechnology Program T32 (5T32GM135066-05; to T.K. and A.H.), support of the Biology of Aging and Age Related Diseases T32 (AG000213; to D.A.B.), and support of an NHGRI training grant to the Genomic Sciences Training Program (5T32HG002760; to D.J.N.). Any opinions, findings, and conclusions or recommendations expressed in this material are those of the author(s) and do not necessarily reflect the views of the National Science Foundation. The content is solely the responsibility of the authors and does not necessarily represent the official views of the National Institutes of Health. The work was also supported in part by startup funds from the University of Wisconsin-Madison School Department of Biochemistry to J.A. Simcox.

AUTHOR CONTRIBUTIONS

Conception, J.W.D., R.J., and J.A. Simcox; methodology, J.W.D., R.J., T.K., G.G., D.J.N., A.A., A.C., K.N., A.H., S.M., X.C., R.V., I.J., K.S., V.H.-G., H.W., D.A.B., G.W., and E.S.; original draft, R.J. and J.A. Simcox; revisions, J.W.D., T.K., R.J., A.C., I.J., and J.A. Simcox; materials, W.-X.D., J.J.C., J.A. Shayman, M.A.-R., and J.A. Simcox; supervision, J.A. Shayman., M.A.-R., and J.A. Simcox.

DECLARATION OF INTERESTS

J.J.C. is a consultant for Thermo Fisher Scientific, 908 Devices, and Seer. M. A.-R. is a scientific advisory board member of Lycia Therapeutics and senior advisor of Scenic Biotech.

STAR★METHODS

Detailed methods are provided in the online version of this paper and include the following:

- KEY RESOURCES TABLE
- EXPERIMENTAL MODEL AND STUDY PARTICIPANT DETAILS
  - Mice
  - In vitro
- METHOD DETAILS
  - Luciferase Assay
  - RNA extraction and RT-PCR
  - ChIP-seq
  - TFEB Immunoprecipitation
  - Western blot
  - Electron microscopy
  - Lipid extraction
  - Untargeted lipidomics
  - Targeted BMP and PG lipid measurements
  - Non-esterified fatty acid measurements
  - Ketone body assay
  - Cathepsin B assay
  - Liposome assay
- QUANTIFICATION AND STATISTICAL ANALYSIS

SUPPLEMENTAL INFORMATION

Supplemental information can be found online at https://doi.org/10.1016/j.cmet.2025.04.015.

Received: November 14, 2023
Revised: January 13, 2025
Accepted: April 21, 2025
Published: May 14, 2025

REFERENCES

1. Bornstein, M.R., Neinast, M.D., Zeng, X., Chu, Q., Axsom, J., Thorsheim, C., Li, K., Blair, M.C., Rabinowitz, J.D., and Arany, Z. (2023). Comprehensive quantification of metabolic flux during acute cold stress in mice. Cell Metab. *35*, 2077–2092.e6. https://doi.org/10.1016/j.cmet.2023.09.002.
2. Chitraju, C., Fischer, A.W., Farese, R.V., Jr., and Walther, T.C. (2020). Lipid droplets in brown adipose tissue are dispensable for cold-induced thermogenesis. Cell Rep. *33*, 108348. https://doi.org/10.1016/j.celrep.2020.108348.
3. Haemmerle, G., Lass, A., Zimmermann, R., Gorkiewicz, G., Meyer, C., Rozman, J., Heldmaier, G., Maier, R., Theussl, C., Eder, S., et al. (2006). Defective lipolysis and altered energy metabolism in mice lacking adipose triglyceride lipase. Science *312*, 734–737. https://doi.org/10.1126/science.1123965.
4. Schreiber, R., Diwoky, C., Schoiswohl, G., Feiler, U., Wongsiriroj, N., Abdellatif, M., Kolb, D., Hoeks, J., Kershaw, E.E., Sedej, S., et al. (2017). Cold-induced thermogenesis depends on ATGL-mediated lipolysis in cardiac muscle, but not brown adipose tissue. Cell Metab. *26*, 753–763.e7. https://doi.org/10.1016/j.cmet.2017.09.004.
5. Jurado-Fasoli, L., Sanchez-Delgado, G., Di, X., Yang, W., Kohler, I., Villarroya, F., Aguilera, C.M., Hankemeier, T., Ruiz, J.R., and Martinez-Tellez, B. (2024). Cold-induced changes in plasma signaling lipids are associated with a healthier cardiometabolic profile independently of

brown adipose tissue. Cell Rep. Med. *5*, 101387. https://doi.org/10.1016/j.xcrm.2023.101387.

6. Simcox, J., Geoghegan, G., Maschek, J.A., Bensard, C.L., Pasquali, M., Miao, R., Lee, S., Jiang, L., Huck, I., Kershaw, E.E., et al. (2017). Global analysis of plasma lipids identifies liver-derived acylcarnitines as a fuel source for brown fat thermogenesis. Cell Metab. *26*, 509–522.e6. https://doi.org/10.1016/j.cmet.2017.08.006.
7. Sostre-Colón, J., Uehara, K., Garcia Whitlock, A.E., Gavin, M.J., Ishibashi, J., Potthoff, M.J., Seale, P., and Titchenell, P.M. (2021). Hepatic AKT orchestrates adipose tissue thermogenesis via FGF21-dependent and -independent mechanisms. Cell Rep. *35*, 109128. https://doi.org/10.1016/j.celrep.2021.109128.
8. Zhang, S., Williams, K.J., Verlande-Ferrero, A., Chan, A.P., Su, G.B., Kershaw, E.E., Cox, J.E., Maschek, J.A., Shapira, S.N., Christofk, H.R., et al. (2024). Acute activation of adipocyte lipolysis reveals dynamic lipid remodeling of the hepatic lipidome. J. Lipid Res. *65*, 100434. https://doi.org/10.1016/j.jlr.2023.100434.
9. Jain, R., Wade, G., Ong, I., Chaurasia, B., and Simcox, J. (2022). Determination of tissue contributions to the circulating lipid pool in cold exposure via systematic assessment of lipid profiles. J. Lipid Res. *63*, 100197. https://doi.org/10.1016/j.jlr.2022.100197.
10. Kirkegaard, T., Roth, A.G., Petersen, N.H.T., Mahalka, A.K., Olsen, O.D., Moilanen, I., Zylicz, A., Knudsen, J., Sandhoff, K., Arenz, C., et al. (2010). Hsp70 stabilizes lysosomes and reverts Niemann-Pick disease-associated lysosomal pathology. Nature *463*, 549–553. https://doi.org/10.1038/nature08710.
11. Locatelli-Hoops, S., Remmel, N., Klingenstein, R., Breiden, B., Rossocha, M., Schoeniger, M., Koenigs, C., Saenger, W., and Sandhoff, K. (2006). Saposin A mobilizes lipids from low cholesterol and high bis(monoacylglycerol)phosphate-containing membranes: patient variant saposin A lacks lipid extraction capacity. J. Biol. Chem. *281*, 32451–32460. https://doi.org/10.1074/jbc.M607281200.
12. Rodriguez-Navarro, J.A., Kaushik, S., Koga, H., Dall'Armi, C., Shui, G., Wenk, M.R., Di Paolo, G., and Cuervo, A.M. (2012). Inhibitory effect of dietary lipids on chaperone-mediated autophagy. Proc. Natl. Acad. Sci. USA *109*, E705–E714. https://doi.org/10.1073/pnas.1113036109.
13. Akgoc, Z., Sena-Esteves, M., Martin, D.R., Han, X., d'Azzo, A., and Seyfried, T.N. (2015). Bis(monoacylglycero)phosphate: a secondary storage lipid in the gangliosidoses. J. Lipid Res. *56*, 1006–1013. https://doi.org/10.1194/jlr.M057851.
14. Medoh, U.N., and Abu-Remaileh, M. (2024). The bis(monoacylglycero)-phosphate hypothesis: from lysosomal function to therapeutic avenues. Annu. Rev. Biochem. *93*, 447–469. https://doi.org/10.1146/annurev-biochem-092823-113814.
15. Showalter, M.R., Berg, A.L., Nagourney, A., Heil, H., Carraway, K.L., 3rd, and Fiehn, O. (2020). The emerging and diverse roles of bis(monoacylglycero) phosphate lipids in cellular physiology and disease. Int. J. Mol. Sci. *21*, 8067. https://doi.org/10.3390/ijms21218067.
16. Ballabio, A., and Bonifacino, J.S. (2020). Lysosomes as dynamic regulators of cell and organismal homeostasis. Nat. Rev. Mol. Cell Biol. *21*, 101–118. https://doi.org/10.1038/s41580-019-0185-4.
17. Settembre, C., De Cegli, R., Mansueto, G., Saha, P.K., Vetrini, F., Visvikis, O., Huynh, T., Carissimo, A., Palmer, D., Klisch, T.J., et al. (2013). TFEB controls cellular lipid metabolism through a starvation-induced autoregulatory loop. Nat. Cell Biol. *15*, 647–658. https://doi.org/10.1038/ncb2718.
18. Varadharajan, V., Ramachandiran, I., Massey, W.J., Jain, R., Banerjee, R., Horak, A.J., McMullen, M.R., Huang, E., Bellar, A., Lorkowski, S.W., et al. (2024). Membrane-bound O-acyltransferase 7 (MBOAT7) shapes lysosomal lipid homeostasis and function to control alcohol-associated liver injury. eLife *12*, RP92243. https://doi.org/10.7554/eLife.92243.
19. Oninla, V.O., Breiden, B., Babalola, J.O., and Sandhoff, K. (2014). Acid sphingomyelinase activity is regulated by membrane lipids and facilitates cholesterol transfer by NPC2. J. Lipid Res. *55*, 2606–2619. https://doi.org/10.1194/jlr.M054528.
20. Laqtom, N.N. (2023). Studying lysosomal function and dysfunction using LysoIP. Nat. Rev. Mol. Cell Biol. *24*, 773. https://doi.org/10.1038/s41580-023-00619-6.
21. Xia, J.Y., Holland, W.L., Kusminski, C.M., Sun, K., Sharma, A.X., Pearson, M.J., Sifuentes, A.J., McDonald, J.G., Gordillo, R., and Scherer, P.E. (2015). Targeted induction of ceramide degradation leads to improved systemic metabolism and reduced hepatic steatosis. Cell Metab. *22*, 266–278. https://doi.org/10.1016/j.cmet.2015.06.007.
22. Longato, L., Tong, M., Wands, J.R., and de la Monte, S.M. (2012). High fat diet induced hepatic steatosis and insulin resistance: Role of dysregulated ceramide metabolism. Hepatol. Res. *42*, 412–427. https://doi.org/10.1111/j.1872-034X.2011.00934.x.
23. Grabner, G.F., Fawzy, N., Schreiber, R., Pusch, L.M., Bulfon, D., Koefeler, H., Eichmann, T.O., Lass, A., Schweiger, M., Marsche, G., et al. (2020). Metabolic regulation of the lysosomal cofactor bis(monoacylglycero) phosphate in mice. J. Lipid Res. *61*, 995–1003. https://doi.org/10.1194/jlr.RA119000516.
24. Sardiello, M., Palmieri, M., di Ronza, A., Medina, D.L., Valenza, M., Gennarino, V.A., Di Malta, C., Donaudy, F., Embrione, V., Polishchuk, R. S., et al. (2009). A gene network regulating lysosomal biogenesis and function. Science *325*, 473–477. https://doi.org/10.1126/science.1174447.
25. Palmieri, M., Impey, S., Kang, H., di Ronza, A., Pelz, C., Sardiello, M., and Ballabio, A. (2011). Characterization of the CLEAR network reveals an integrated control of cellular clearance pathways. Hum. Mol. Genet. *20*, 3852–3866. https://doi.org/10.1093/hmg/ddr306.
26. Azimifar, S.B., Nagaraj, N., Cox, J., and Mann, M. (2014). Cell-type-resolved quantitative proteomics of murine liver. Cell Metab. *20*, 1076–1087. https://doi.org/10.1016/j.cmet.2014.11.002.
27. Niu, L., Geyer, P.E., Gupta, R., Santos, A., Meier, F., Doll, S., Wewer Albrechtsen, N.J., Klein, S., Ortiz, C., Uschner, F.E., et al. (2022). Dynamic human liver proteome atlas reveals functional insights into disease pathways. Mol. Syst. Biol. *18*, e10947. https://doi.org/10.15252/msb.202210947.
28. Gosis, B.S., Wada, S., Thorsheim, C., Li, K., Jung, S., Rhoades, J.H., Yang, Y., Brandimarto, J., Li, L., Uehara, K., et al. (2022). Inhibition of nonalcoholic fatty liver disease in mice by selective inhibition of mTORC1. Science *376*, eabf8271. https://doi.org/10.1126/science.abf8271.
29. Abu-Remaileh, M., Wyant, G.A., Kim, C., Laqtom, N.N., Abbasi, M., Chan, S.H., Freinkman, E., and Sabatini, D.M. (2017). Lysosomal metabolomics reveals V-ATPase- and mTOR-dependent regulation of amino acid efflux from lysosomes. Science *358*, 807–813. https://doi.org/10.1126/science.aan6298.
30. Eapen, V.V., Swarup, S., Hoyer, M.J., Paulo, J.A., and Harper, J.W. (2021). Quantitative proteomics reveals the selectivity of ubiquitin-binding autophagy receptors in the turnover of damaged lysosomes by lysophagy. eLife *10*, e72328. https://doi.org/10.7554/eLife.72328.
31. Yu, Y., Gao, S.M., Guan, Y., Hu, P.-W., Zhang, Q., Liu, J., Jing, B., Zhao, Q., Sabatini, D.M., Abu-Remaileh, M., et al. (2024). Organelle proteomic profiling reveals lysosomal heterogeneity in association with longevity. eLife *13*, e85214. https://doi.org/10.7554/eLife.85214.
32. Bouley, R.A., Hinkovska-Galcheva, V., Shayman, J.A., and Tesmer, J.J.G. (2019). Structural basis of lysosomal phospholipase A2 inhibition by Zn2+. Biochemistry *58*, 1709–1717. https://doi.org/10.1021/acs.biochem.8b01124.
33. Glukhova, A., Hinkovska-Galcheva, V., Kelly, R., Abe, A., Shayman, J.A., and Tesmer, J.J.G. (2015). Structure and function of lysosomal phospholipase A2 and lecithin:cholesterol acyltransferase. Nat. Commun. *6*, 6250. https://doi.org/10.1038/ncomms7250.
34. Burke, J.E., and Dennis, E.A. (2009). Phospholipase A2 structure/function, mechanism, and signaling. J. Lipid Res. *50*, S237–S242. https://doi.org/10.1194/jlr.R800033-JLR200.
35. Shayman, J.A., and Tesmer, J.J.G. (2019). Lysosomal phospholipase A2. Biochim. Biophys. Acta Mol. Cell Biol. Lipids *1864*, 932–940. https://doi.org/10.1016/j.bbalip.2018.07.012.

36. Abe, A., Hiraoka, M., and Shayman, J.A. (2007). The acylation of lipophilic alcohols by lysosomal phospholipase A2. J. Lipid Res. *48*, 2255–2263. https://doi.org/10.1194/jlr.M700277-JLR200.

37. Abe, A., Hiraoka, M., and Shayman, J.A. (2006). Positional specificity of lysosomal phospholipase A2. J. Lipid Res. *47*, 2268–2279. https://doi.org/10.1194/jlr.M600183-JLR200.

38. Grabner, G.F., Fawzy, N., Pribasnig, M.A., Trieb, M., Taschler, U., Holzer, M., Schweiger, M., Wolinski, H., Kolb, D., Horvath, A., et al. (2019). Metabolic disease and ABHD6 alter the circulating bis(monoacylglycerol)phosphate profile in mice and humans. J. Lipid Res. *60*, 1020–1031. https://doi.org/10.1194/jlr.M093351.

39. Anderson, D.M.G., Ablonczy, Z., Koutalos, Y., Hanneken, A.M., Spraggins, J.M., Calcutt, M.W., Crouch, R.K., Caprioli, R.M., and Schey, K.L. (2017). Bis(monoacylglycero)phosphate lipids in the retinal pigment epithelium implicate lysosomal/endosomal dysfunction in a model of Stargardt disease and human retinas. Sci. Rep. *7*, 17352. https://doi.org/10.1038/s41598-017-17402-1.

40. Body, D.R., and Gray, G.M. (1967). The isolation and characterisation of phosphatidylglycerol and a structural isomer from pig lung. Chem. Phys. Lipids *1*, 254–263. https://doi.org/10.1016/0009-3084(67)90032-1.

41. Scherer, M., Schmitz, G., and Liebisch, G. (2010). Simultaneous quantification of cardiolipin, bis(monoacylglycero)phosphate and their precursors by hydrophilic interaction LC–MS/MS including correction of isotopic overlap. Anal. Chem. *82*, 8794–8799. https://doi.org/10.1021/ac1021826.

42. Boland, S., Swarup, S., Ambaw, Y.A., Malia, P.C., Richards, R.C., Fischer, A.W., Singh, S., Aggarwal, G., Spina, S., Nana, A.L., et al. (2022). Deficiency of the frontotemporal dementia gene GRN results in gangliosidosis. Nat. Commun. *13*, 5924. https://doi.org/10.1038/s41467-022-33500-9.

43. Logan, T., Simon, M.J., Rana, A., Cherf, G.M., Srivastava, A., Davis, S.S., Low, R.L.Y., Chiu, C.L., Fang, M., Huang, F., et al. (2021). Rescue of a lysosomal storage disorder caused by Grn loss of function with a brain penetrant progranulin biologic. Cell *184*, 4651–4668.e25. https://doi.org/10.1016/j.cell.2021.08.002.

44. Bulfon, D., Breithofer, J., Grabner, G.F., Fawzy, N., Pirchheim, A., Wolinski, H., Kolb, D., Hartig, L., Tischitz, M., Zitta, C., et al. (2024). Functionally overlapping intra- and extralysosomal pathways promote bis(monoacylglycero)phosphate synthesis in mammalian cells. Nat. Commun. *15*, 9937. https://doi.org/10.1038/s41467-024-54213-1.

45. Medoh, U.N., Hims, A., Chen, J.Y., Ghoochani, A., Nyame, K., Dong, W., and Abu-Remaileh, M. (2023). The Batten disease gene product CLN5 is the lysosomal bis(monoacylglycero)phosphate synthase. Science *381*, 1182–1189. https://doi.org/10.1126/science.adg9288.

46. Singh, S., Dransfeld, U.E., Ambaw, Y.A., Lopez-Scarim, J., Farese, R.V., and Walther, T.C. (2024). PLD3 and PLD4 synthesize S,S-BMP, a key phospholipid enabling lipid degradation in lysosomes. Cell *187*, 6820–6834.e24. https://doi.org/10.1016/j.cell.2024.09.036.

47. Alvarez-Valadez, K., Sauvat, A., Diharce, J., Leduc, M., Stoll, G., Guittat, L., Lambertucci, F., Paillet, J., Motiño, O., Ferret, L., et al. (2024). Lysosomal damage due to cholesterol accumulation triggers immunogenic cell death. Autophagy *21*, 934–956. https://doi.org/10.1080/15548627.2024.2440842.

48. Ilnytska, O., Lai, K., Gorshkov, K., Schultz, M.L., Tran, B.N., Jeziorek, M., Kunkel, T.J., Azaria, R.D., McLoughlin, H.S., Waghalter, M., et al. (2021). Enrichment of NPC1-deficient cells with the lipid LBPA stimulates autophagy, improves lysosomal function, and reduces cholesterol storage. J. Biol. Chem. *297*, 100813. https://doi.org/10.1016/j.jbc.2021.100813.

49. Taniyama, Y., Shibata, S., Kita, S., Horikoshi, K., Fuse, H., Shirafuji, H., Sumino, Y., and Fujino, M. (1999). Cloning and expression of a novel lysophospholipase which structurally resembles lecithin cholesterol acyltransferase. Biochem. Biophys. Res. Commun. *257*, 50–56. https://doi.org/10.1006/bbrc.1999.0411.

50. Hinkovska-Galcheva, V., Kelly, R., Manthei, K.A., Bouley, R., Yuan, W., Schwendeman, A., Tesmer, J.J.G., and Shayman, J.A. (2018). Determinants of pH profile and acyl chain selectivity in lysosomal phospholipase A(2). J. Lipid Res. *59*, 1205–1218. https://doi.org/10.1194/jlr.M084012.

51. Nyame, K., Xiong, J., de Jong, A.P., Alsohybe, H.N., Raaben, M., Hartmann, G., Simcox, J.A., Blomen, V.A., and Abu-Remaileh, M. (2024). PLA2G15 is a lysosomal BMP hydrolase with ester position specificity and its targeting ameliorates lysosomal disease. Preprint at bioRxiv. https://doi.org/10.1101/2024.06.07.597919.

52. Chen, J., Cazenave-Gassiot, A., Xu, Y., Piroli, P., Hwang, R., DeFreitas, L., Chan, R.B., Di Paolo, G., Nandakumar, R., Wenk, M.R., et al. (2023). Lysosomal phospholipase A2 contributes to the biosynthesis of the atypical late endosome lipid bis(monoacylglycero)phosphate. Commun. Biol. *6*, 210. https://doi.org/10.1038/s42003-023-04573-z.

53. Abe, A., Hinkovska-Galcheva, V., Bouchev, P., Bouley, R., and Shayman, J.A. (2024). The role of lysosomal phospholipase A2 in the catabolism of bis(monoacylglycerol)phosphate and association with phospholipidosis. J. Lipid Res. *65*, 100574. https://doi.org/10.1016/j.jlr.2024.100574.

54. Chen, S., Francioli, L.C., Goodrich, J.K., Collins, R.L., Kanai, M., Wang, Q., Alföldi, J., Watts, N.A., Vittal, C., Gauthier, L.D., et al. (2024). A genomic mutational constraint map using variation in 76,156 human genomes. Nature *625*, 92–100. https://doi.org/10.1038/s41586-023-06045-0.

55. Kagohashi, Y., Sasaki, M., May, A.I., Kawamata, T., and Ohsumi, Y. (2023). The mechanism of Atg15-mediated membrane disruption in autophagy. J. Cell Biol. *222*, e202306120. https://doi.org/10.1083/jcb.202306120.

56. Li, Y., Wang, X., Li, M., Yang, C., and Wang, X. (2022). M05B5.4 (lysosomal phospholipase A2) promotes disintegration of autophagic vesicles to maintain C. elegans development. Autophagy *18*, 595–607. https://doi.org/10.1080/15548627.2021.1943178.

57. Nyame, K., Hims, A., Aburous, A., Laqtom, N.N., Dong, W., Medoh, U.N., Heiby, J.C., Xiong, J., Ori, A., and Abu-Remaileh, M. (2024). Glycerophosphodiesters inhibit lysosomal phospholipid catabolism in Batten disease. Mol. Cell *84*, 1354–1364.e9. https://doi.org/10.1016/j.molcel.2024.02.006.

58. Severgnini, M., Sherman, J., Sehgal, A., Jayaprakash, N.K., Aubin, J., Wang, G., Zhang, L., Peng, C.G., Yucius, K., Butler, J., et al. (2012). A rapid two-step method for isolation of functional primary mouse hepatocytes: cell characterization and asialoglycoprotein receptor based assay development. Cytotechnology *64*, 187–195. https://doi.org/10.1007/s10616-011-9407-0.

STAR★METHODS

KEY RESOURCES TABLE

REAGENT or RESOURCE	SOURCE	IDENTIFIER
Antibodies		
Rabbit anti-Pla2g15	Novus Biologicals	NBP2-17193
Rabbit anti-TFEB (western blot)	Bethyl Laboratories	A303-673A; RRID: AB_11204751
Tfeb polyclonal antibody	Proteintech	13372-1-AP; RRID: AB_2199611
TFEB rabbit mAb (IP)	Cell Signaling	83010; RRID: AB_3105800
LC3B Antibody	Cell Signaling	2775; RRID: AB_915950
Normal Rabbit IgG	Cell Signaling	2729; RRID: AB_1031062
Phospho-(Ser/Thr) Phe Antibody	Cell Signaling	9631; RRID: AB_330308
Histone H3 (1B1B2) Mouse mAb	Cell Signaling	14269; RRID: AB_2756816
Rab5a polyclonal antibody	Proteintech	11947-1-AP; RRID: AB_2269388
LIPA polyclonal antibody	Proteintech	12956-1-AP; RRID: AB_2078477
CD107B/LAMP2 monoclonal antibody	Proteintech	66301-1-Ig; RRID: AB_2881684
Human/mouse/rat beta-actin antibody	R&D Systems	MAB8929; RRID: AB_3076436
Recombinant anti-HNF-4-alpha antibody	Abcam	ab181604; RRID: AB_2890918
Anti-LAMP1	Development Studies Hybridoma Bank, Iowa	1D4B; RRID: AB_2134500
Goat anti-Rabbit IgG Secondary antibody HRP	Fisher Scientific	PI32460
Goat anti-Mouse IgG Secondary antibody HRP	ThermoFisher Scientific	A-10668; RRID: AB_2534058
Goat anti-Rat IgG Secondary antibody HRP	Fisher Scientific	A10549; RRID: AB_10561556
Chemicals, peptides, and recombinant proteins		
Splash II Lipidomix	Avanti Polar Lipids	330709
14:0 BMP (S, R)	Avanti Polar Lipids	857131
18:1 BMP (S, R)	Avanti Polar Lipids	857133
18:1 (delta-9-cis) PG	Avanti Polar Lipids	840475
15:0-18:1-d7-PG	Avanti Polar Lipids	791640
15:0-18:1-d7-PA	Avanti Polar Lipids	791642
C15 Ceramide-d7 (d18:1-d7/15:0)	Avanti Polar Lipids	860681
Stearic acid-d35	Cayman Chemical	9003318
Oleoyl-L-carnitine-d3 (chloride)	Cayman Chemical	26578
Pierce Formic Acid, LC-MS Grade	ThermoFisher Scientific	85178
Acetonitrile	Honeywell	LC015
Ammonium Formate	Honeywell	55674
Water B&J Brand, LC-MS	Fisher Scientific	600-30-78
Fisher Chemical Isopropanol Optima, LC-MS	Fisher Scientific	A4614
DMEM	ThermoFisher Scientific	11-965-118
Fetal Bovine Serum (FBS)	ThermoFisher Scientific	10-437-028
DPBS	ThermoFisher Scientific	14190144
Lipofectamine RNAiMAX	ThermoFisher Scientific	13778030
Opti-MEM	ThermoFisher Scientific	31985062
Laemmli sample buffer	Bio-Rad	161-0737
β-mercaptoethanol	Sigma-Aldrich	M6250
RIPA lysis buffer	Fisher-Scientific	NC984499

(*Continued on next page*)

Continued

REAGENT or RESOURCE	SOURCE	IDENTIFIER
Pierce protease inhibitor mini tablets, EDTA free	Fisher-Scientific	PIA32955
4-15% Mini-Protean TGX precast protein gels	Bio-Rad	4561096
PowerUp SYBR Green Master Mix	ThermoFisher Scientific	A25778
TRIzol	Invitrogen	15596018
Cathepsin B substrate III – Fluorogenic, Calbiochem	Millipore Sigma	219392
E-64-D	Enzo Life Sciences	BML-PI107-0001
Isoflurane 99.9%	McKesson	803250
25% glutaraldehyde	Electron Microscopy Sciences	16220
0.4M Sodium cacodylate	Electron Microscopy Sciences	11655
Critical commercial assays		
Glucosylceramidase activity assay kit	Abcam	ab273339
β-Hydroxybutyrate colorimetric assay kit	Cayman Chemical	700190
Wako HR Series NEFA kit	Fujifilm	999-34691; 995-34791; 991-34891; 993-35191; 276-76491; 997-76491
SimpleChIP Plus kit (Magnetic Beads) 4°C and RT reagents	Cell Signaling	#38191
Pierce Protein A/G Magnetic Beads	VWR	PI88802
Pierce BCA Protein Assay	ThermoFisher Scientific	#23225
High Capacity cDNA Reverse Transcription Kit	ThermoFisher Scientific	#4368813
Zymo ChIP DNA Clean and Concentrator Kit	VWR	D5205
Qubit dsDNA HS Assay Kit	ThermoFisher Scientific	Q32851
Agilent DNA HS Kit	Agilent Technologies	5067-4626
TruSeq ChIP Sample Preparation kit	Illumina	IP-202-1012
SuperSignal West Atto Ultimate Sensitivity Substrate	ThermoFisher Scientific	A38554
Deposited data		
Untargeted lipidomics data (WT mice)	https://doi.org/10.1016/j.jlr.2022.100197	MTBLS3730
Targeted LC/MS lipidomics data	This paper	ftp://massive.ucsd.edu/v06/MSV000096791/
TFEB ChIP-seq	This paper	GEO: GSE292817
Experimental models: Cell lines		
Hepa1-6 cells	ATCC	CRL-1830
Experimental models: Organisms/strains		
Mouse: C57BL/6J male mice 9 weeks	Jackson Laboratories	#000664
Oligonucleotides		
ON-TARGETplus Mouse Tfeb siRNA	Dharmacon	L-050607-02-0005
ON-TARGETplus Non-targeting Control Pool	Dharmacon	D-001810-10-05
ON-TARGETplus Mouse Pla2g15 siRNA	Dharmacon	L-059873-01-0005
Primers see Table S1	N/A	N/A
Recombinant DNA		
AAV8-GFP-U6-scrmb-shRNA	Vector Biolabs	220207-220729
AAV8-GFP-U6-mTFEB-shRNA	Vector Biolabs	220801#38
Software and algorithms		
R version 4.3.0	R Core team	https://www.r-project.org

(*Continued on next page*)

Continued		
REAGENT or RESOURCE	SOURCE	IDENTIFIER
Agilent MassHunter Suite	Agilent Technologies	G3337AA; M5960AA; M6010AA
Agilent LipidAnnotator	Agilent Technologies	G3835AA
LipidCreator	Peng et al.	https://doi.org/10.1038/s41467-020-15960-z
R scripts for data analysis	This paper	Github: RJain52/Hepatic-TFEB
Other		
TissueLyser II	Qiagen	85300
Tecan Infinite M Plex	Tecan	30190085
QuantStudio 5 Real-Time PCR System	ThermoFisher Scientific	A34322
Acquity UPLC BEH C18 Column	Waters Corporation	186002352
Acquity UPLC BEH C18 VanGuard Pre-Column	Waters Corporation	1860003975
Agilent 1290 Infinity II LC System	Agilent Technologies	N/A
Agilent 6495c triple quadrupole mass spectrometer	Agilent Technologies	G6495CA
Agilent 6546 Q-TOF mass spectrometer	Agilent Technologies	G6546AA
iBright CL1500 Imaging System	ThermoFisher Scientific	A44240
Amersham Protran nitrocellulose blotting membrane	Fisher	45004003
Physitemp rectal probe for mouse	Fisher	NC9713069
JEM 1016CX electron microscope	JEOL Ltd.	N/A
Formulab Diet	LabDiet	5008

EXPERIMENTAL MODEL AND STUDY PARTICIPANT DETAILS

Mice

Mouse husbandry

All animal experiments were performed in accordance with institutional guidelines and were approved by the Institutional Animal Care and Use Committee at the University of Wisconsin-Madison. Mice were housed at room temperature (21-24°C), with relative humidity ranging from 30-50% with an average of 37%, using 12hr dark and 12hr light cycles. Mice had *ad libitum* access to water and standard chow diet (Rodent Diet 5001) prior to experiments. Age, sex, and treatment are specified in each figure legend. *Pla2g15* control *(Pla2g15*$^{+/+}$*)* and knockout *(Pla2g15*$^{-/-}$*)* mice were maintained as litter mate controls through breeding heterozygous mice (*Pla2g15*$^{+/-}$). Genotyping was performed at 21 days, on tail clipping, by Transnetyx using previously published methods and primers, 5′-CAGGGTAGCTCACAACTCTTTG-3′; b, 5′-CAAAGCTCTGGACTGTTTTCCTGC-3′; c, 5’-GAATTCCTAGACCCCAGCAAGAGGAATGTG-3′; and d, 5′-CCCTCCCCAGAGATGGATATTT-3′.[36,37] LysoTag mice were maintained in accordance with the Institutional Animal Care and Use Committee at Stanford University.[20]

Cold tolerance test

Mice were placed without bedding at room temperature (RT; 22°C) or cold (4°C), food was removed at the start of the experiment, and mice had *ad libitum* access to water (n=5-6/group). Temperature was taken hourly via rectal probe and mice were monitored for any changes in behavior or physiology. Experiments started at zeitgeber time=3. At the end of the CTT (cold tolerance test), isoflurane was administered and mice were euthanized post-anesthesia via cervical dislocation. Plasma was obtained via cardiac puncture; post-euthanasia tissue was harvested, washed with PBS, sectioned and either flash frozen in liquid nitrogen or further processed. Hepatocyte isolations were performed immediately following the CTT following standard procedure.[58]

AAV injection

For WT, *Tfeb* KD, *Pla2g15* KD, and *Pla2g15* KO experiments, littermate controls were used and mice were age and weight-matched. Mice were retro-orbitally injected with the appropriate AAV at 1e11 genome copies/mouse (mice weighing 23-28g). Post-injection weights were monitored to ensure no deviation between groups and that no more than 20% body weight was lost post-injection. Subsequent experiments were performed three week after injections.

In vitro

Cell culture

Hepa1-6 cells were cultured at 5% CO_2 at 37°C. Cells were maintained in DMEM with 4.5 g/L glucose, supplemented with 10% fetal bovine serum (FBS). For knockdown of *Tfeb* and *Pla2g15*, ON-TARGETplus Mouse Tfeb pooled siRNA was purchased from Horizon

Discovery. Transfection was performed in Hepa1-6 cells in a 6-well plate using 50 pmol siRNA and Lipofectamine RNAiMAX according to the manufacturer's instructions. Briefly, 5 x 10^5 cells were plated per well in a 6-well culture plate. Cells were cultured in DMEM+10% FBS overnight. The next day, media was replenished and a mixture of 300μL Opti-MEM with 9uL lipofectamine agent and appropriate siRNA was added to wells. Media was replenished 24h later to remove siRNA, then harvested after an additional 24h of culturing.

Generation of Pla2g15 knockout and overexpression cell lines

Knockouts were generated in Hek 293T cells using a CRISPR-Cas9 lentiviral system. Briefly 5 x 10^6 cells were transfected with the helper plasmids pVSVg, pMDLgRRE, pRSV-rev and the pLenti plasmids containing either the *Pla2g15* guide or a GFP control. Transfection was carried out using the Lipofectamine 3000 reagent (Thermo Scientific #L3000008). After 2 days virus was harvested, filtered through a 0.45μm syringe filter and 1μL of 10mg/mL polybrene was added per mL of media harvested. Virus was added to Hek 293T cells and selected for puromycin resistance (3μL of 10mg/mL puro per 10mL of media) after 3 days. For *Pla2g15* overexpression in the knockout cell lines, PhoA cells were grown to 80% confluence and transfected with pBABE plasmids and PEI transfection reagent. After 2 days virus was harvested, filtered through a 0.45μm syringe filter and 10mg/mL polybrene was added at 1:1000 dilution. Virus was added to 293T cells and selected for hygromycin resistance (200μg/mL).

METHOD DETAILS

Luciferase Assay

Potential TFEB binding sites were identified from ChIP data and aligned with mm10 reference genome (chr8: 106143980-106151020). This sequence was divided into 5 regions of ∼1500bp, with ∼100bp overlap and each region was cloned into a pGL3 Basic luciferase reporter plasmid (pGL3 Pla2g15 R1-R5). 293T cells overexpressing *LacZ* or *Tfeb* were generated using a lentiviral system (pLenti-CMV). These 293T cells were plated in 96-well plates and transfected with pGL3 Basic empty vector, *pPparg* (addgene#8896), or pGL3 *Pla2g15* R1-R5, and pCMV-Renilla control plasmid (addgene#118066). After 48h of growth at 37°C, Dual-Glo Luciferase Assay System (Promega, E2940) was used to assess luciferase and Renilla activity. Final activity was expressed as Luciferase Activity/Renilla Activity.

RNA extraction and RT-PCR

RNA was recovered from tissues or cells with Trizol reagent followed by homogenization using TissueLyser. cDNA was synthesized using High-Capacity cDNA Reverse Transcription Kit. RT-PCR amplification was performed for 40 cycles in a 384-well plate using PowerUp SYBR Green Master Mix and the QuantStudio 5 Real-Time PCR System. Primer sequences are listed in Table S1. For quantification, a standard curve was generated for each primer set and used to determine relative gene expression. Expression levels are presented relative to the housekeeping gene *Rps3*.

ChIP-seq

Chromatin immunoprecipitation was performed on livers from individually housed male C57BL/6J mice (11 weeks old) that were placed at 4°C without food for 6 hours or kept at RT with *ad libitum* access to food (n=2 per group). All mice had *ad libitum* access to water. SimpleChIP Plus Enzymatic Chromatin IP Kit was used according to manufacturer's instructions. Briefly, 100mg of tissue was used per mouse and two immunoprecipitations were performed with rabbit anti-TFEB antibody, and two were performed with normal rabbit IgG control. ChIP DNA was purified using Zymo ChIP DNA Clean and Concentrator Kit. Purified immunoprecipitated and input DNA was quantified and assessed for sheering using the Qubit dsDNA HS Assay Kit and Agilent DNA HS chip, respectively. Samples were prepared according the TruSeq ChIP Sample Preparation kit. Libraries were size selected for an average insert size of 350 bp using SPRI-based bead selection. Quality and quantity of the finished libraries were assessed using an Agilent Tapestation and Qubit dsDNA HS Assay Kit, respectively. Paired end 150bp sequencing was performed on the NovaSeq 6000 by the UW-Madison Biotechnology Center.

Sequenced reads were checked for: sequencing quality, insert length, read concordance, duplications, and adapters via FastP and then aligned to the mouse genome (UCSC build mm10) via bowtie2 v2.2.5 using the sensitive end-to-end read alignment mode. Aligned reads were sorted and indexed with SAMtools 1.9 and peaks were called at $p \leq 0.05$ and $q \leq 0.05$ (separately) using the input/IgG as the background control with the MACS2. Primary and differential peaks were annotated for their positioning relative to genomic elements with Homer v4.11. *De novo* and known motif analyses were carried out with Homer. Pathway ontology information was generated by inputting genes differentially bound in cold and RT into https://geneontology.org/ for 'Reactome' pathway results.

TFEB Immunoprecipitation

Liver (100mg) was homogenized in RIPA buffer with protease and phosphatase inhibitors using the TissueLyser II in round-bottom microcentrifuge tubes with a single steel bead. Homogenate was centrifuged at 4°C for 15min at 16000 RPM and the supernatant was transferred to a new tube. This process was repeated to pellet additional cell debris. Protein concentration was measured by BCA assay, and 1mg of protein was aliquoted into low protein-binding tubes with 1uL anti-TFEB antibody (Proteintech 13372-1), 5μL anti-histone H3, or anti IgG. Volume was adjusted to 500μL with RIPA buffer, and samples were mixed overnight at 4°C.

Protein A/G magnetic beads were then added to the samples, which were allowed to mix for 4 hours at 4°C. Beads were washed in RIPA buffer. For Western blot, beads were resuspended in Laemmli Sample Buffer with 5% β-mercaptoethanol and heated at 95°C for 5min. Beads were removed, and the sample was transferred to low protein-binding tubes and stored at -20°C until use. For proteomics, beads were washed again in 20mM Tris 100mM NaCl pH 8, and then resuspended in 100μL 20mM Tris 100mM NaCl pH 8 and stored at -80°C until use.

Western blot

Tissue (25-50mg) was homogenized in a round bottom microfuge tubes containing a single steel bead in RIPA buffer with protease inhibitor using the TissueLyser II. Lysate was centrifuged at 4°C for 10min at 14000 RPM and the supernatant was transferred to a new tube. BCA assay was used to determine protein concentration, then samples were prepared at a concentration of 2mg/mL in Laemmli sample buffer containing 5% β-mercaptoethanol. Samples were heated at 95°C for 5min, then 15-30μg protein were loaded into precast gels. Gels were run at 150V for 30-45min, then transferred at 100V for 75min onto nitrocellulose membranes.

Membranes were blocked in either 5% milk or 5% BSA, per manufacturer instructions, prior to overnight incubation in the appropriate primary antibody at 1:1000 dilution in blocking buffer, overnight at 4°C. Secondary antibodies were diluted at 1:5000 in blocking buffer and incubation was performed for 1h at RT, then membranes were developed using ECL reagent. Blots were imaged and densitometry was performed on an iBright CL1500 imaging system.

Electron microscopy

Mice were sacrificed using isoflurane and cervical dislocation, the liver was immediately perfused with 30mL PBS, followed by the fixation buffer containing 2.5% glutaraldehyde in 0.4M sodium cacodylate (pH=7.4). The liver was excised, submerged in fixation buffer, and cut into small pieces before being placed in fresh fixation buffer overnight at 4°C. The following day, samples were transferred to 15mL tube containing fresh fixation buffer and further processed for imaging. Images were collected on a JEM 1016CX electron microscope.[55]

Lipid extraction

Murine tissues were extracted for lipids using a one-phase method as previously described.[6] For liver, 25-30mg tissue were homogenized in ceramic bead tubes in a 3:1:6 IPA:H_2O:$EtOAc^-$ solution containing the following internal standards (IS): 12μL of SPLASH II LipidoMix and 10μl of 10μM PG 15:0/18:1_{d7}, 10μM BMP 14:0_14:0, 30μM Cer d18:1_15:0_{d7}, 30μM ACar 18:1_{d3}, 225μM C18:0_{d35}, and 1.1mM PA 15:0/18:1_{d7}. A TissueLyser II was used for bead beating. Homogenates were incubated at -20°C for 10min, then centrifuged at 16,000xg for 10min at 4°C to precipitate protein before the lipid containing solvent layer was transferred to a new tube. Samples were respun as previously to precipitate remaining debris, transferred to another tube, then dried down in a SpeedVac. Lipid extracts were resuspended in 150μl 100% MeOH for negative or 9:1 MeOH:toluene for positive ionization analysis. Plasma samples were extracted identically except 50μl plasma were used as starting material. Samples were transferred into autosampler vials containing glass inserts for analysis.

Samples from cell culture were prepared by first aspirating media, washing twice with DPBS on ice, then gently scraping cells into 1mL DPBS and transferring to a microfuge tube. After pelleting the samples and aspirating DPBS, 100% MeOH containing IS as above was added to samples for lipid extraction. Cell pellets were dispersed with light vortexing and incubated on ice for 1h, with additional vortexing every 15min. Following centrifugation at 16,000xg for 15min to pellet proteins and cell debris, the lipid containing liquid phase was transferred to a new tube. Extracts were respun to pellet remaining debris, then transferred to autosampler vials with inserts for analysis.

Untargeted lipidomics

Lipid extracts were analyzed as previously described.[6] Briefly, an Agilent 1290 Infinity II liquid chromatograph (LC) coupled to an Agilent 6546 quadrupole time-of-flight mass spectrometer (MS) was used for untargeted analyses. Lipids were separated using a Waters Acquity BEH C18 column (1.7μm, 2.1x100mm) held at 50°C. Mobile phase A was 60:40 MeCN:H_2O and B was 9:1:90 MeCN:H_2O:IPA, both with 0.1% (v/v) formic acid and 10mM ammonium formate, using the following gradient: 15% mobile phase B to 30% at 2.40min, to 48% at 3min, to 82% at 13.2min, finally to 99% from 13.2 to 13.8min held until 15.4 min before re-equilibration to 15% at a constant 0.500mL/min. Samples were analyzed in positive and negative ionization mode as separate experiments. All samples were injected undiluted at 10μl volumes for negative mode. For positive ionization, samples were diluted 20 to 40-fold (after evaluating saturation) and injected with a volume between 1–3μL.

Libraries of identified lipids were created using pooled samples and collecting MS/MS spectra on 6 consecutive injections using iterative exclusion. Agilent LipidAnnotator was used for lipid annotation, then individual samples were analyzed using MS1 acquisition and peak integration was performed in Agilent Profinder using mass and retention time from the lipid libraries. Subsequent steps including normalization to IS were performed in R using publicly available custom scripts (https://github.com/RJain52/Multi-Tissue-Cold-Exposure-Lipidomics).

Targeted BMP and PG lipid measurements

A targeted BMP and PG LC/MS method was developed using an Agilent 1290 Infinity I LC coupled to an Agilent 6495c triple-quadrupole MS. Lipids were extracted using a one-phase extraction (see lipid extraction).[34,38] An *in-silico* multiple reaction monitoring

(MRM) method was developed using LipidCreator for fragmentation patterns of BMP and PG of different acyl chain configurations in positive ($[M+H]^+$ and $[M+NH4]^+$ adducts) and negative ($[M-H]^-$) ionization modes.[56] Samples were then injected using the same LC parameters as described in the untargeted lipidomics section using the MRM methods. BMP lipids eluted 0.3-1min earlier than the PG species of the same acyl chains, depending on the species. This pattern was confirmed using BMP 18:1_18:1 and PG 18:1_18:1 standards purchased from Avanti Polar Lipids. Additionally, BMP(s) had unique fragments in positive ionization mode when compared to PG(s) of the same species. No unique fragments were observed in negative ionization mode; however the acyl chain carbon lengths were discernable, and ion signals were much higher due to the physicochemical properties of BMP and PG. Therefore, we created a negative mode dynamic MRM (dMRM) method for all identifiable BMP and PG species using retention time information from positive ionization mode, in which we could distinguish isomeric BMP and PG species via fragmentation, but scanning for precursor/products providing acyl chain information. For all subsequent analyses, pooled extracts were run in positive and negative ionization modes to allow for manual verification of lipid identity and individual samples were run only using negative mode dMRM analysis. Non-endogenous BMP 14:0/14:0 and PG 15:0/18:1_{d7} were used as IS. Data was processed in Agilent MassHunter Quantitative Analysis prior to downstream analyses in R.

Non-esterified fatty acid measurements

Liver non-esterified fatty acids were measured using a colorimetric assay on a Tecan plate reader according to manufacturer's instructions. A five-point standard curve (0∼2.5 mM) of non-esterified oleic acid standard was used to calculate NEFA concentration from 2μl plasma. Samples were analyzed in duplicate.

Ketone body assay

Plasma ketone bodies were measured by colorimetric assay using the manufacturer protocol. Briefly, 40μl plasma were diluted with 60μl assay buffer then duplicate wells for each sample were prepped with 50μl diluted plasma/well. Reaction was initiated and allowed to run for 30min at RT in the dark, then read using a Tecan plate reader at a wavelength of 445nm.

Cathepsin B assay

Cathepsin B was assayed as previously described.[30] Briefly, 15mg liver was homogenized in 300μl lysis buffer (50mM Tris, 130mM NaCl, 10% (v/v) glycerol, 0.5% (v/v) NP-40, 0.5mM EDTA, 0.5mM EGTA, 1mM PMSF; pH=7.4) using sonication (Branson Sonifier 450) (60% duty cycle; output=4) on ice. Protein content was measured using BCA assay, then 15ug protein was incubated with 50uM cathepsin B substrate. Reactions were conducted in the presence and absence of the cathepsin B inhibitor E-64-D in assay buffer (100mM NaCl, 100mM sodium acetate; pH=5.5) at a final volume of 100μl for 30min at 37°C. Activity was based on fluorescence of cleaved substrate measured at an excitation/emission of 355/460nm.

Liposome assay

Liposome assays were carried out as previously described.[57] Briefly, S,S-(3,3'-di$C_{18:1}$)-BMP/1,2-*O*-dioctadecenyl-*sn*-glycero-3-phosphocholine (DODPC, non-substrate of Pla2g15) liposomes were prepared by mixing reagents in a glass tube and drying down under N_2. Lipid mixture was dispersed in a 50mM sodium acetate solution (pH 4.5) using sonication. To avoid the possibility of diisopropyl fluorophosphate (DFP) affecting lipid membranes, DFP-treated PLA2G15 was dialyzed against 0.25 M sucrose/25 mM Hepes (pH 7.4)/1 mM EDTA before use. The UV spectrum of DFP-treated PLA2G15 after dialysis was compared to DFP-untreated PLA2G15 to confirm the structural properties of the protein. There was no significant difference in the spectra between the DFP-conjugated PLA2G15 and the untreated PLA2G15. Reactions contained liposomes and either sucrose buffer, sucrose buffer with human PLA2G15, or sucrose buffer with DFP-treated human PLA2G15, incubated at 37°C for 10min. Reactions were quenched with 2:1 chloroform:MeOH (2:1, v/v), then 0.9% (w/v) NaCl solution causing phase separation of a top aqueous and bottom hydrophobic layer. The bottom hydrophobic layer was transferred to glass tubes, dried down under N_2, and developed using thin-layer chromatography with a solvent system of chloroform:MeOH:pyridine (99:1:2, v/v) to separate lipid fractions. Bands corresponding to lipid fractions were visualized by heating the plate treated with 8% (w/v) $CuSO_4$ solution with 6.8% (v/v) H_3PO_4 and 32% (v/v) MeOH.[57]

QUANTIFICATION AND STATISTICAL ANALYSIS

Analyses were conducted using R unless otherwise stated. Where relevant, mean±SD were reported. For comparisons between two groups, Student's t-test was used and a *p-value* less than 0.05 was considered significant, unless otherwise stated. For untargeted analyses, false-discovery correction $q<0.05$ was considered significant. For comparisons of >2 groups, ANOVA analysis was used to test for significance followed by pairwise t-tests. All scripts used for analysis are freely available on Github (username: RJain52).